INVESTIGATION OF ELECTRON–ATOM/MOLECULE SCATTERING RESONANCES USING COMPLEX MULTICONFIGURATIONAL SELF-CONSISTENT FIELD METHOD

A Dissertation

by

KOUSIK SAMANTA

Submitted to the Office of Graduate Studies of
Texas A&M University
in partial fulfillment of the requirements for the degree of

DOCTOR OF PHILOSOPHY

May 2009

Major Subject: Chemistry

INVESTIGATION OF ELECTRON–ATOM/MOLECULE SCATTERING RESONANCES USING COMPLEX MULTICONFIGURATIONAL SELF-CONSISTENT FIELD METHOD

A Dissertation

by

KOUSIK SAMANTA

Submitted to the Office of Graduate Studies of
Texas A&M University
in partial fulfillment of the requirements for the degree of

DOCTOR OF PHILOSOPHY

Approved by:

Chair of Committee,	Danny L. Yeager
Committee Members,	Roland E. Allen
	Michael B. Hall
	Robert R. Lucchese
Head of Department,	David H. Russell

May 2009

Major Subject: Chemistry

ABSTRACT

Investigation of Electron–Atom/Molecule Scattering Resonances Using Complex Multiconfigurational Self-Consistent Field Method. (May 2009)

Kousik Samanta, B.Sc., University of Calcutta, India;

M.Sc., Indian Institute of Technology Bombay, India

Chair of Advisory Committee: Dr. Danny L. Yeager

We present a complex multiconfigurational self-consistent field (CMCSCF)–based approach to investigate electron–atom/molecule scattering resonances. A modified second quantization algebra adapted for biorthogonal spin orbitals has been applied to develop a quadratically convergent CMCSCF scheme. A new step-length control algorithm has been introduced in order to control the walk on the complex energy hypersurface and converge to correct CMCSCF stationary point. We have also developed a method (M_1 method) based on the multiconfigurational spin tensor electron propagator (MCSTEP) to calculate resonance energies directly.

These methods have been applied to investigate atomic and molecular scattering resonances. The test cases for our application were ^2P Be^- and $^2\Pi_g$ N_2^- shape resonances. The position and the width of these resonances have been calculated for different complete active space choices. Convergence for CMCSCF calculations to a tolerance of 1.0×10^{-10} a.u. for the energy gradient is achieved typically within ten iterations or less. The wide distribution of the values for the position and the width of the resonance reported in the literature has been explained by showing that there actually exists two distinct resonances which are close in energy. The resonance positions and widths from our calculation for the $^2\Pi_g$ N_2^- shape resonance have been found to be very close to the experimental results. In another study, the effect of the orbitals with higher angular momentum has been investigated.

To my parents and my wife

ACKNOWLEDGMENTS

I would like to thank my advisor, Professor Danny Yeager, for his constant help and support during my career as a graduate student and researcher. Had he not been there to help me with my small and not–so–small problems in every wake of my research none of the work presented here would have taken shape. His knowledge, wisdom and experience have always been a source of inspiration for me.

Thanks are also due to Dr. Dongxia Ma whose comments, suggestions and advice often helped me solve new problems and come up with a totally different point of view for the old ones.

I am also grateful to Professor Manoj Mishra from Indian Institute of Technology Bombay who inspired me to start working in this field in the first place.

I would like to express my sincere and humble gratitude to Mr. Mrinmaya Samanta and Mr. Pranab Samanta, my teachers in the early days of my education, who also happen to be my cousins. They are the ones who inspired me to look at everything with a scientist's eye.

I would also like to thank my parents for their unconditional love and care and for being there for me at every stage of my life.

Thanks are due to my parents–in–law as well, who have always been a constant source of love, support and motivation.

Last but not the least, I would like to thank my lovely wife, Moumita for being at my side always and motivating me all the way along.

TABLE OF CONTENTS

CHAPTER Page

LIST OF TABLES

LIST OF FIGURES

FIGURE Page

CHAPTER I

INTRODUCTION

In the last two centuries, scattering experiments with electrons as projectiles became very popular in unraveling the mystery of atoms and molecules. These experiments involve the creation of electron–atom/molecule resonances which are metastable continuum states. These transient species are found to play major roles in diverse processes involving electron transport and energy exchange between electronic and nuclear motions. They are also involved in the vibrational excitation of molecules or molecular ions by electron impact, the dissociative attachment and recombination which are processes of great importance in the outer space, the higher atmosphere and plasmas and discharges.[1,2] In addition to that, the mechanism for DNA damage by low–energy electrons has recently been reported to involve these resonances.[3]

For the past few decades the challenge of theoretically investigating the resonances that occur in the electron-atom/molecule. scattering experiments using low-energy electron beam has attracted attention[4–19] Although the resonances lie in the continuum part of the Hamiltonian buried under the non-resonant scattering states, their *quasi-bound* nature appealed to many theoreticians to apply bound state methods to study them. The first purely bound state approach was the stabilization method.[4,20,21] However, the complex scaling theorem[5–7] developed in the early 1970s by Aguilar, Balslev, Combes and Simon has been found to be one of the most convenient ways to apply bound state methods.

This dissertation follows the style of the *Journal of the American Chemical Society.*

The complex scaling theorem states that if the electronic coordinates ($\mathbf{r}$) of the Hamiltonian are scaled ("dilated") by a complex parameter $\eta = \alpha \exp(i\theta)$ as $\eta\mathbf{r}$, where α and θ are real numbers, the continua is rotated by an angle of -2θ at each threshold, exposing the resonances hidden in the continua. The complex eigenvalues of the dilated Hamiltonian correspond to the scattering states (including the resonant scattering states), although the bound states and the ionization and the excitation thresholds remain real and unmodified.

In the conventional complex scaling method, originally introduced for the cases involving dilatation analytic potentials,[5–7] $\mathbf{r}$ is scaled regardless of its magnitude, r. With a view to avoid problems involving non-dilatation–analytic potentials, two other scaling schemes were introduced by Moiseyev and coworkers, viz. exterior complex scaling[22] and smooth–exterior complex scaling,[23] which are based on Simon's proposal[24] of keeping the electronic coordinates on the real axis long enough to avoid non-analiticities. McCurdy and Rescigno introduced the idea of the complex basis functions instead of scaling the Hamiltonian.[9,25] The complex absorbing potential (CAP) technique[14] which has some *formal* connections with the smooth–exterior complex scaling,[26,27] has gained attention in recent years.[17–19,28]

In this study we implement the conventional complex scaling technique using the quadratically convergent multiconfigurational self-consistent field method (MCSCF) which will be referred to as CMCSCF. The motivation for this comes from the facts that (1) MCSCF is a very efficient method to describe non-dynamical and some dynamical correlations correctly[29–35] (2) MCSCF is computationally much cheaper than full configuration interaction calculations,[32] (3) the quadratically convergent MCSCF scheme powered by an efficient step-length control algorithm facilitates fast convergence to the desired stationary point,[36] (4) conventional complex scaling is the most straightforward way to do a complex scaling calculation with least amount of

modification of the existing bound state codes and also has an extensive and successful history, and (5) to our knowledge, the method of conventional scaling using MCSCF has not been used along with the step–length control algorithm (see Reference 37 for the first implementation).

This study involves implementation of CMCSCF, development of a constrained optimization algorithm for CMCSCF, development of the M_1 method based on the first block of the M matrix defined in multiconfigurational spin–tensor electron propagator,[33] and their applications in the investigation of atomic and molecular scattering resonances. We begin by giving a brief overview of the complex scaling theorem and its implications in Chapter I. Chapter II deals with the implementation of CMCSCF and development of the constrained optimization algorithm and application of CMCSCF to study ^2P Be^- shape resonances. In Chapter III, the development of M_1 method is discussed along with the application of the same to study ^2P Be^- shape resonances. Chapter IV includes discussions about the effect of expanding the complete active space size in CMCSCF to include orbitals with higher angular momentum. Our first application of our CMCSCF based M_1 method to study molecular resonances is discussed in Chapter V. At the end we conclude and summarize our discussion.

CHAPTER II

THE COMPLEX SCALING METHOD AND ITS APPLICATION

A. Introduction

Resonances are temporarily bound metastable states which lie in the continuum part of the Hamiltonian. The quasi-bound nature of these states prompted many theoreticians to apply bound–state based methods. The complex scaling theorem developed by Aguilar, Balslev and Combes[5,6] and Simon[7] has been proved to be one of the best ways to apply a bound–state method to study resonances.

In this chapter we develop the necessary theoretical framework for the complex scaling method (CSM) and show how it can be used with bound state methods. In the next section we give a brief outline on the origin of the divergent resonance wavefunction in the Siegert's treatment.[38] Next, we introduce the complex scaling transformation necessary to bring the resonance wavefunction and the Hamiltonian to a useful form. After that we discuss the change in the spectrum of the complex scaled Hamiltonian upon complex scaling transformation and how resonances hidden in the continuum can be uncovered. In the next section we discuss the problem associated with using a finite basis sets. We also give an overview of the trajectory method of searching resonances using a finite basis set. Next we introduce the concept of biorthogonality in connection with the complex scaled Hamiltonian, which is followed by a discussion about the modified second quantization algebra required to deal with the biorthogonality. Then we discuss about some computational aspects of the CSM, especially how the different parts of the complex scaled Hamiltonian may be constructed. At the end we conclude and summarize our discussion.

B. Scattering Resonances and Divergent Siegert Function

According to Dirac[39,40] and Gamow,[41] the time development of the metastable resonance states may be described by

$$\Psi(\mathbf{r},t) = \psi(\mathbf{r})\exp(-iEt/\hbar) \tag{2.1}$$

with

$$E = E_r - i\Gamma/2, \quad E_r \in \mathbb{R},\ \Gamma \in \mathbb{R}, \tag{2.2}$$

where E_r is the "position" of the resonance and Γ is its "width" which is related to its lifetime (τ) by the uncertainty relation

$$\Gamma = \hbar/\tau. \tag{2.3}$$

It is evident that the provision for complex E leaves the possibility of having a finite lifetime.

The use of time–dependent Schrödinger equation (TDSE),

$$i\hbar\frac{\partial}{\partial t}\Psi(\mathbf{r},t) = \hat{\mathcal{H}}\Psi(\mathbf{r},t) \tag{2.4}$$

leads to the time–independent Schrödinger equation (TISE),

$$\hat{\mathcal{H}}\psi(\mathbf{r}) = E\psi(\mathbf{r}), \tag{2.5}$$

which is similar to the ordinary TISE in regular quantum mechanics except for the complex E. Real Hermitian Hamiltonians ($\hat{\mathcal{H}}$) cannot have complex eigenvalues,

and hence the states with complex E remain "hidden" in the continuum part of the Hamiltonian.

Siegert[38] showed that scattering resonance wavefunctions can be obtained by solving Eq. (2.5) subject to the constraint that there is no incoming waves [of the form $\exp(-ikr)$ with $k^2 = 2mE/\hbar^2$] for $r \to \infty$. However, the Siegert resonance wavefunction which is of the form

$$\psi_{\rm res}(\mathbf{r}) \sim \exp(ikr) \tag{2.6}$$

diverges asymptotically since[42]

$$\exp(ikr) = \exp(iKr\cos\beta)\exp(Kr\sin\beta) \tag{2.7}$$

where $k = K\exp(-\beta)$, $K = |k|$, and $0 < \beta < \pi/2$. The range of β values comes from the fact that the *physical* scattering events correspond to $\mathrm{Re}(k) > 0$ and the scattering resonances lie in the fourth quadrant of the complex k plane if the behavior of the S matrix in terms of k is considered.[43] Hence, the Siegert function is not square–integrable, i.e. $\psi_{\rm res} \notin \mathscr{L}^2$.

In order to apply a bound state method, we must use an unbounded similarity transformation, u, which will make the wavefunctions convergent, i.e.

$$\lim_{r\to\infty} u\psi_{\rm res} = 0 \tag{2.8}$$

as well as change the spectrum of Hamiltonian as

$$\left(u\hat{\mathcal{H}}u^{-1}\right)(u\psi_{\rm res}) = (E_r - i\Gamma/2)(u\psi_{\rm res}) \tag{2.9}$$

to allow for complex eigenvalues.[44,45]

C. The Complex Scaling Transformation

Following Löwdin's development,[44] the complex scaling transformation, $u(\eta)$ is defined for a function f of a real or a complex variable z as[5–7]

$$u(\eta)f(z) = \eta^{1/2} f(\eta z) \tag{2.10}$$

where the parameter η is a complex scale factor, which can be conveniently expressed in terms of two real parameters α ($\alpha > 0$) and θ as

$$\eta = \alpha \exp(i\theta) \tag{2.11}$$

It can be shown[44] that $u(\eta)$ is an unbounded similarity transformation and the transformed Hamiltonian

$$\hat{H} = u(\eta)\hat{\mathcal{H}}u^{-1}(\eta) \tag{2.12}$$

is non-Hermitian and complex symmetric

$$\hat{H}^{\dagger} = \hat{H}^{*} \neq \hat{H}. \tag{2.13}$$

and hence permits complex eigenvalues.

The complex scaling transformation essentially results in the scaling of the electronic coordinates of the Hamiltonian, $\mathbf{r}$ to $\eta\mathbf{r}$. A straight-forward application of Eq. (2.10) and Eq. (2.12) by making use of the following important property of the

transformation

$$u^{-1}(\eta) = u(\eta^{-1}), \tag{2.14}$$

one can see that the kinetic ($\hat{T}$) and potential energy parts ($\hat{V}$) of the Hamiltonian are scaled as

$$\hat{T} \rightarrow \eta^{-2}\hat{T} \tag{2.15}$$

$$\hat{V} \rightarrow \eta^{-1}\hat{V} \tag{2.16}$$

for an atomic systems. The complex scaling of the electron-nuclear potential for a molecular system is a little more complicated and it is discussed in Section H of this chapter as well as in Chapter VI.

In order to investigate the effect of this transformation on the bound and the continuum states, we start by transforming a bound state wavefunction of the form $\exp(-\kappa r) \in \mathscr{L}^2$ ($\kappa > 0$) as

$$\begin{aligned} u(\eta)\exp(-\kappa r) &= \eta^{1/2}\exp(-\kappa\eta r) \\ &= \eta^{1/2}\exp(-\kappa\alpha r\cos\theta)\exp(-i\kappa\alpha r\sin\theta). \end{aligned} \tag{2.17}$$

It is evident that the transformed wavefunction is still square–integrable for $\theta \in [-\pi/2, \pi/2]$ and hence it fulfills the same boundary conditions as the unscaled function. Because the eigenvalues are determined by the boundary conditions, they (the eigenvalues) remain unaltered.

On the other hand, a continuum wavefunction, e.g. the Siegert function de-

scribed in Eq. (2.6), is transformed under complex scaling as

$$\begin{aligned} u(\eta)\exp(ikr) &= \eta^{1/2}\exp(ik\eta r) \\ &= \eta^{1/2}\exp[iKr\alpha\cos(\theta-\beta)]\exp[-Kr\alpha\sin(\theta-\beta)] \end{aligned} \tag{2.18}$$

which is $\mathscr{L}^2$–type if $0 \leq \theta - \beta \leq \pi$, i.e. $\theta \in [\beta, \pi + \beta]$.

However, $\theta \in (\pi/2, \pi + \beta]$, a subset of the above domain of θ values that make the continuum functions convergent, causes the bound state wavefunctions to diverge. Hence, in order to obtain $\mathscr{L}^2$–type wavefunctions for both the bound and the continuum states simultaneously, $\theta \in [\beta, \pi/2]$. The critical value, $\theta_c = \beta$ is system–specific.

D. Spectrum of the Complex Scaled Hamiltonian

If the potential vanishes sufficiently rapidly at $r \to \infty$, and is otherwise well-behaved, the kinetic energy part $\eta^{-2}\hat{T}$ becomes the dominant contribution in the continuum part of the spectrum, which is moved by an angle -2θ in the complex energy plane (to the fourth quadrant). According to the general theory of complex scaling,[5–7] the discrete energy eigenvalues of the ground state and the low–lying excited states will be *persistent* eigenvalues, whereas the *new eigenvalues* associated with physical resonances may be revealed in the complex plane as the "continuum ray" is made to pass through them by means of increasing the angle θ (see Figure 1).

This makes way for complex eigenvalues ("new eigenvalues") which were *hidden* in the continua before the scaling, in addition to the persistent real eigenvalues which correspond to the bound states and the ionization and the excitation thresholds.

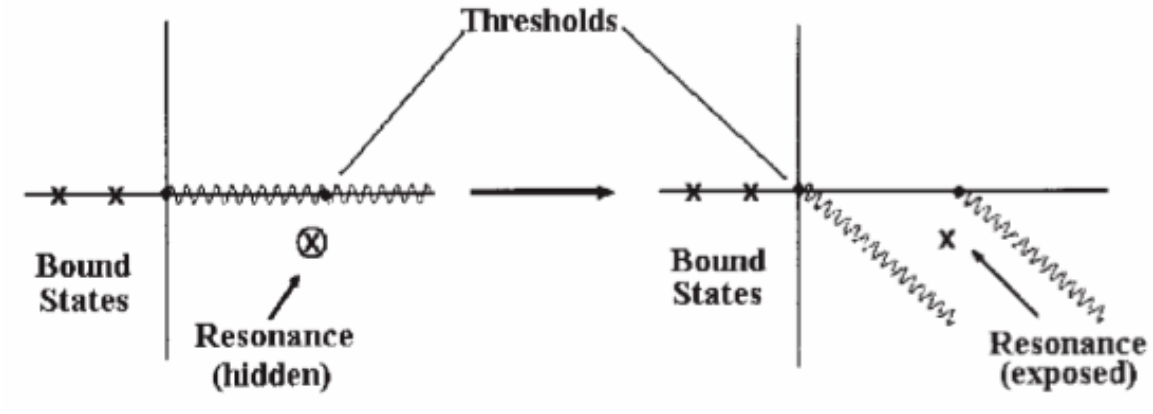

Figure 1. Change in the spectrum on complex scaling $\hat{\mathcal{H}} \rightarrow \hat{H}$. The x and y axes represent $\mathrm{Re}(E)$ and $\mathrm{Im}(E)$, respectively.

For $\theta > \theta_c$ the eigenvalue, $E(\eta)$ corresponding to a resonance behaves like a persistent eigenvalue and becomes independent of the complex scale factor, η:

$$\frac{d^m E}{d\eta^m} = 0; \quad \theta > \theta_c;\ m = 1, 2, 3, \cdots . \tag{2.19}$$

The corresponding eigenfunction is $\mathscr{L}^2$–type. The persistent nature of the resonance eigenvalues for $\theta > \theta_c$ causes the resonances to stand out among other non-resonant scattering states, and the square–integrability of the resonance eigenfunctions in this region thus makes way for the employment of a bound state method to investigate the resonances. The complex analogue of the variational principle[10,46,47] ensures that one can search for a stationary point in the complex energy hypersurface using a bound state method.

E. Trajectory Method and Calculation of the Resonance Energy

Eq. (2.19) holds true if an *infinite* basis set is used, but in an actual calculation only a *finite* basis set can be used. The use of a finite basis set makes the resonance energy, $E(\theta > \theta_c)$, depend on η; and only a *quasi-stability* in a very narrow neighborhood of some

$$\eta = \eta_o = \alpha_o \exp(i\theta_o) \tag{2.20}$$

obtained by solving

$$\frac{dE(\eta)}{d\eta} = 0, \tag{2.21}$$

indicates the appearance of the resonance.[10] $E(\eta_o)$ is taken as the best estimate for the resonance energy in a practical calculation. Eq. (2.21) implies that

$$\left(\frac{\partial E}{\partial \theta}\right)_{\alpha=\alpha_o} = i\eta \left(\frac{\partial E}{\partial \eta}\right)_{\alpha=\alpha_o} = 0 \tag{2.22}$$

and

$$\left(\frac{\partial E}{\partial \alpha}\right)_{\theta=\theta_o} = \left(\frac{\eta}{\alpha}\right) \left(\frac{\partial E}{\partial \eta}\right)_{\theta=\theta_o} = 0 \tag{2.23}$$

which form the basis of trajectory method[10,48,49] of determining $E(\eta_o)$ by inspecting the stability (loops, kinks, inflexion or any kind of "slowing down") in the plots of $\mathrm{Im}(E(\eta))$ as a function of $\mathrm{Re}(E(\eta))$ at a series of constant α ("θ-trajectory") and constant θ ("α-trajectory") values until a self-consistency in $E(\eta_o)$ is achieved.

Resonance energy is traditionally reported as the total energy of the resonant state relative to that of the bound state target. If we define a quantity, $\varepsilon(\eta) = E_c^{N\pm1}(\eta) - E_b^N$, which is the energy of the $(N \pm 1)$-electron continuum state relative to that of the N-electron bound state (b and c indicate bound and continuum states, respectively), then we can rewrite Eqs. (2.21), (2.22) and (2.23) by substituting E with ε since E_b^N is independent of variations in η, and thus identify $\varepsilon(\eta_o)$ as the resonance energy. We redefine the position and the width of the resonance in terms of $\varepsilon(\eta_o)$ as

$$\varepsilon(\eta_o) = E_r - i\Gamma/2. \tag{2.24}$$

F. The Biorthogonality of the Eigenfunctions of the Hamiltonian

Following Löwdin's formulation,[44] if we define a pair of non-self-adjoint operators, $\hat{\mathcal{O}}$ having an eigenfunction C associated with the eigenvalue λ and $\hat{\mathcal{O}}^T$ having

an eigenfunction D associated with the eigenvalue μ such that

$$\begin{aligned} \hat{\mathcal{O}} &= \hat{\mathcal{O}}^T, \quad \text{where } \hat{\mathcal{O}}^T \equiv \hat{\mathcal{O}}^{\dagger *}, && (2.25)\\ \hat{\mathcal{O}}C &= \lambda C, && (2.26)\\ \hat{\mathcal{O}}^T D &= \mu D, && (2.27) \end{aligned}$$

then

$$\begin{aligned} \lambda\langle D^*|C\rangle &= \langle D^*|\hat{\mathcal{O}}|C\rangle \\ &= \langle \hat{\mathcal{O}}^\dagger D^*|C\rangle \\ &= \langle (\hat{\mathcal{O}}^T D)^*|C\rangle \\ &= \mu\langle D^*|C\rangle \\ \implies (\lambda-\mu)\langle D^*|C\rangle &= 0. \end{aligned} \tag{2.28}$$

So, if $\lambda \neq \mu$, then one obtains the biorthogonality relation

$$\langle D^*|C\rangle = 0; \quad \lambda \neq \mu, \tag{2.29}$$

and if $\langle D^*|C\rangle \neq 0$ then λ must be equal to μ. So, in general, after proper normalization we obtain the *biorhonormality* relation as

$$\langle D^*|C\rangle = \delta_{\mu\lambda}. \tag{2.30}$$

Another important feature of these two operators is that they have the same set of eigenfunctions which can be seen from the following by comparing it with

Eq. (2.26) for $\mu = \lambda$:

$$\hat{\mathcal{O}}D = \hat{\mathcal{O}}^T D = \mu D = \lambda D \tag{2.31}$$

$$\implies D = C. \tag{2.32}$$

Similarly, the complex scaled Hamiltonian and its transpose, i.e. $\hat{H}$ and $\hat{H}^T$, which are also non-self-adjoint with the property $\hat{H} = \hat{H}^T$, also have a common set of *biorthogonal* eigenfunctions.

G. Modified Second Quantization Algebra for Biorthogonal Spin-Orbitals

The biorthogonality of the eigenfunctions of the complex scaled Hamiltonian can be expressed as

$$\langle \psi_i^* | \psi_j \rangle = \int_{\text{all space}} \psi_i \psi_j d\tau = \delta_{ij}, \tag{2.33}$$

where it is assumed that the wavefunctions are normalized to unity. It is a common practice in electronic structure calculation methods to express the wavefunctions (eigenfunctions of $\hat{H}$) in terms of Slater determinants comprising spin-orbitals in order to preserve antisymmetry. However, the biorthogonality of the wavefunctions requires that the Slater determinants be biorthogonal which in turn mandates the biorthogonality of the spin-orbitals, $\{\varphi_p\}$, i.e.

$$\langle \varphi_p^* | \varphi_q \rangle = \delta_{pq}. \tag{2.34}$$

The MCSCF equations are based on the second quantization algebra based on an orthogonal set of spin-orbitals. The biorthogonality of the spin-orbitals in the

current study demands a modification on the second quantization algebra itself.[50]

The modified second quantization algebra may be introduced by using creation operators (a_p^T) in the same way as Jørgensen and Simon[30] by showing the correspondence between an N-electron Slater determinant, $(N!)^{-1/2}\det|\varphi_p\varphi_q\cdots\varphi_r\cdots\varphi_s|$, and a ket containing N spin-orbitals generated by acting N creation operators, $a_p^T, a_q^T, \cdots, a_r^T, \cdots, a_s^T$ on the hypothetical vacuum ket, $|\text{vac}\rangle$, as

$$a_s^T\cdots a_r^T\cdots a_q^T a_p^T|\text{vac}\rangle \longleftrightarrow (N!)^{-1/2}\det|\varphi_p\varphi_q\cdots\varphi_r\cdots\varphi_s|. \tag{2.35}$$

The use of "T" (for "transpose"), instead of "†" (for "Hermitian conjugate"), in the creation operators stems from the biorthogonality of the spin-orbitals.

The action of a creation operator, a_p^T, on an arbitrary ket may be viewed as a creation of an electron in a spin-orbital, φ_p, in the ket with proper change in sign to account for the Pauli principle if φ_p is unoccupied and zero if it was already occupied. On the other hand, an annihilation operator, a_p, may be viewed as an operator which removes an electron from φ_p in the ket with proper sign change in accordance with Pauli principle if φ_p is occupied, and gives rise to zero otherwise. These may be expressed algebraically in terms of the ket in Eq. (2.35), which has φ_r occupied but φ_t empty:

$$\begin{aligned}
a_t^T\left(a_s^T\cdots a_r^T\cdots a_q^T a_p^T|\text{vac}\rangle\right) &= a_t^T a_s^T\cdots a_r^T\cdots a_q^T a_p^T|\text{vac}\rangle \\
&= (-1)^{k_t} a_s^T\cdots a_r^T\cdots a_t^T\cdots a_q^T a_p^T|\text{vac}\rangle \qquad (2.36)\\
a_r^T\left(a_s^T\cdots a_r^T\cdots a_q^T a_p^T|\text{vac}\rangle\right) &= 0 \qquad (2.37)\\
a_r\left(a_s^T\cdots a_r^T\cdots a_q^T a_p^T|\text{vac}\rangle\right) &= (-1)^{k_r} a_s^T\cdots\cdots a_q^T a_p^T|\text{vac}\rangle \qquad (2.38)\\
a_t\left(a_s^T\cdots a_r^T\cdots a_q^T a_p^T|\text{vac}\rangle\right) &= 0 \qquad (2.39)
\end{aligned}$$

Equations (2.36) and (2.38), where k_t and k_r are the number of creation operators standing in the left of a_t^T and a_r^T in the original ket, respectively, indicate how the Pauli principle is taken into account. The roles of these operators are switched when they act on a bra instead. The properties of these operators may be best understood by looking at their anticommutation relations:

$$\{a_p^T, a_q^T\} = a_p^T a_q^T + a_q^T a_p^T = 0 \tag{2.40}$$

$$\{a_p, a_q\} = a_p a_q + a_q a_p = 0 \tag{2.41}$$

$$\{a_p^T, a_q\} = a_p^T a_q + a_q a_p^T = \delta_{pq} \tag{2.42}$$

All the quantum mechanical operators that appear in first quantization have second quantization analogues. The second quantization equivalents for one- and two-electrons operators in the first quantization notation, e.g. $\sum_{i=1}^{N} f(\mathbf{r}_i)$ and $\sum_{i,j=1}^{N} g(\mathbf{r}_i, \mathbf{r}_j)$ are

$$\sum_{i=1}^{N} f(\mathbf{r}_i) \longleftrightarrow \sum_{p,q} \langle \varphi_p^* | f | \varphi_q \rangle a_p^T a_q \tag{2.43}$$

and

$$\sum_{i,j=1}^{N} g(\mathbf{r}_i, \mathbf{r}_j) \longleftrightarrow \sum_{p,q,r,s} \langle \varphi_p^* \varphi_q^* | g | \varphi_r \varphi_s \rangle a_p^T a_q^T a_s a_r \tag{2.44}$$

where the sums (p, q) and (p, q, r, s) run over a complete set of biorthogonal spin-orbitals.

H. Construction of the Complex Scaled Hamiltonian

The scaling $\mathbf{r} \rightarrow \eta \mathbf{r}$ causes the kinetic energy and the electron–nuclear attractive and the electron–electron repulsive potentials for an atomic system to be scaled

as [see Eqs. (2.15) and (2.16)]

$$-(1/2)\nabla^2 \rightarrow -(1/2)\eta^{-2}\nabla^2, \tag{2.45}$$

$$-Zr^{-1} \rightarrow -Z\eta^{-1}r^{-1}, \tag{2.46}$$

$$r_{12}^{-1} \rightarrow \eta^{-1}r_{12}^{-1} \tag{2.47}$$

(in atomic units), respectively, where Z is the nuclear positive charge and r_{12} is the distance between electrons 1 and 2. These indicate that the complex integrals required to construct the complex scaled Hamiltonian may be calculated by first calculating the integrals over basis functions (real) using a real integral evaluation program and then transforming them to integrals over orbitals by multiplying them with the orbital–expansion coefficients (complex, in general), which are then multiplied by appropriate complex factors as indicated above. Hence, the complex scaled electronic Hamiltonian for an atomic system may now be expressed as[50]

$$\hat{H} = \sum_{p,q} h_{pq}\, a_p^T a_q + \sum_{p,q,r,s} V_{pqrs}\, a_p^T a_q^T a_s a_r \tag{2.48}$$

where the one- and two-body integrals are given by

$$h_{pq} = -(1/2)\eta^{-2}\langle\varphi_p^*|\nabla^2|\varphi_q\rangle - Z\eta^{-1}\langle\varphi_p^*|r^{-1}|\varphi_q\rangle \tag{2.49}$$

and

$$V_{pqrs} = (1/2)\eta^{-1}\langle\varphi_p^*(1)\varphi_q^*(2)|r_{12}^{-1}|\varphi_r(1)\varphi_s(2)\rangle, \tag{2.50}$$

respectively (in atomic units).

However, in case of molecules, the integrals involving the electron–nuclear

attractive potential which is scaled as

$$-\frac{Z_A}{|\mathbf{r}-\mathbf{R}_A|} \rightarrow -\frac{Z_A}{|\eta\mathbf{r}-\mathbf{R}_A|} \tag{2.51}$$

($\mathbf{R}_A$ represents the coordinates of the nucleus of an atomic center with nuclear positive charge Z_A) must be evaluated for each η from scratch since the electronic coordinates are not independent of the nuclear coordinate system. The concern about the analiticity of the electron–nuclear potential and the convergence of the corresponding integrals were addressed by McCurdy and Rescigno[51] and Moiseyev and Corcoran[52] who also gave a prescription for evaluating these integrals. These were followed up by the electron propagator (EP) calculations of Donnelly and coworkers[53] and Mishra and coworkers.[54–57]

I. Summary and Conclusions

In this chapter an outline of the theoretical development of the complex scaling method (CSM) is given. The discussion in this chapter is the background for our development of multiconfigurational self-consistent field based methods to investigate resonances.

First, an introduction about the divergent resonance wavefunction in connection with the Siegert method is given. This is followed by the introduction of the complex scaling transformation that makes the wavefunctions convergent and the Hamiltonian permit complex eigenvalues which are representative of the continuum states. The transformation which is essentially the scaling of all the electronic coordinates by a complex parameter rotates the continuum part of the complex scaled

Hamiltonian and the resonances are uncovered as the rotated continuum ray is made to pass through them by means of changing the scale factor. The resonance eigenvalues are persistent which helps to identify the resonances among a myriad of non-resonant scattering states. However, for a finite basis set that persistence is not so strong, and the resonances may be discovered by using a trajectory method which is based on systematically changing the scale factor.

The complex scaling has some other conceptual implications as well, for example, the eigenfunctions of the complex scaled Hamiltonian are biorthogonal which requires the use of a modified second quantization algebra based on a set of biorthogonal spin orbitals.

A discussion on how to calculate the complex scaled integrals for in order to construct the complex scaled Hamiltonian for atomic and molecular systems is included at then end.

CHAPTER III

INVESTIGATION OF SCATTERING RESONANCES: A COMPLEX MULTICONFIGURATIONAL SELF-CONSISTENT FIELD APPROACH

A. Introduction

In this study we implement the complex scaling method[5–7] under the framework of multiconfigurational self consistent field theory (MCSCF). The quadratically convergent MCSCF method[29,36,58] is an excellent electronic structure calculation method which accounts for most of the non-dynamic and some dynamic correlations. The theoretical background of MCSCF using CSM (which will be referred to as "CMCSCF") was developed by Yeager et al.[50]

The original quadratically convergent MCSCF scheme uses a "guaranteed convergence" algorithm developed by Jørgensen et al.[36] which enhances convergence of an MCSCF calculation to the correct stationary point. A similar algorithm to control the walk on the complex energy hypersurface has been developed in this study. The CMCSCF was applied to study the ^2P Be^- shape resonance positions and widths.

In the next section, the theoretical development of quadratically convergent CMCSCF and the step–length control algorithm is discussed. After that, we present our results and at then we summarize and conclude our discussion.

B. Theory

1. A Quadratically Convergent CMCSCF Scheme

Yeager et al.[50] developed a quadratically convergent complex multiconfigurational self-consistent field method (CMCSCF), i.e. MCSCF using the complex scaled Hamiltonian ($\hat{H}$), which may be described in terms of an orthogonal transformation of the state $|0\rangle$ to the optimized state $|\tilde{0}\rangle$:[50,59]

$$\exp(\hat{\kappa})\exp(\hat{S})|0\rangle = |\tilde{0}\rangle \tag{3.1}$$

where

$$\hat{\kappa} = \sum_{p>q} \kappa_{pq}\hat{Q}_{pq} \;\text{ with }\; \hat{Q}_{pq} = a_p^T a_q - a_q^T a_p\,, \tag{3.2}$$

and

$$\hat{S} = \sum_{n\neq 0} S_{n0}\hat{R}_n \;\text{ with }\; \hat{R}_n = |n\rangle\langle 0^*| - |0\rangle\langle n^*|. \tag{3.3}$$

In Eq. (3.3), the states $\{|n\rangle\}$ belong to the orthogonal complement space of $|0\rangle$. In practice the coefficients $\{\kappa_{pq}(p>q)\}$ and $\{S_{n0}(n\neq 0)\}$ are packed as column vectors ($\underline{\kappa}$ and $\underline{S}$, respectively), which are again arranged in another column vector known as step–length vector,

$$\underline{\lambda} = \begin{pmatrix} \underline{\kappa} \\ \underline{S} \end{pmatrix}. \tag{3.4}$$

The total energy of the optimized state may be written as a Taylor series in terms of the step–length vector, $\underline{\lambda}$, the first derivative vector, $\underline{F}$ and the Hessian, $\underline{\underline{G}}$ as

$$E(\underline{\lambda}) = \langle\tilde{0}^*|\hat{H}|\tilde{0}\rangle = E(\underline{0}) + \underline{\lambda}^T\underline{F} + \tfrac{1}{2}\underline{\lambda}^T\underline{\underline{G}}\,\underline{\lambda} + \cdots \tag{3.5}$$

$$\Rightarrow E(\underline{\lambda}) \approx q(\underline{\lambda}) = E(\underline{0}) + \underline{\lambda}^T\underline{F} + \tfrac{1}{2}\underline{\lambda}^T\underline{\underline{G}}\,\underline{\lambda}\ , \tag{3.6}$$

where

$$E(\underline{0}) = \langle 0^*|\hat{H}|0\rangle; \tag{3.7}$$

$$\underline{F} = \begin{pmatrix} \underline{F}_\kappa \\ \underline{F}_S \end{pmatrix} \tag{3.8}$$

with the elements

$$(\underline{F}_\kappa)_{pq} = \langle 0^*|[\hat{H}, \hat{Q}_{pq}]|0\rangle, \tag{3.9}$$

and

$$(\underline{F}_S)_n = \langle 0^*|[\hat{H}, \hat{R}_n]|0\rangle; \tag{3.10}$$

$$\underline{\underline{G}} = \begin{pmatrix} \underline{\underline{G}}_{\kappa\kappa} & \underline{\underline{G}}_{\kappa S} \\ \underline{\underline{G}}_{S\kappa} & \underline{\underline{G}}_{SS} \end{pmatrix} \tag{3.11}$$

with the following elements

$$\left(\underline{\underline{G}}_{\kappa\kappa}\right)_{pq,tu} = \left(\underline{\underline{G}}_{\kappa\kappa}\right)_{tu,pq} = -\langle 0^*|[\hat{Q}_{pq}, \hat{H}, \hat{Q}_{tu}]|0\rangle, \tag{3.12}$$

$$\left(\underline{\underline{G}}_{\kappa S}\right)_{pq,n} = \left(\underline{\underline{G}}_{S\kappa}\right)_{n,pq} = -\langle 0^*|[\hat{R}_n, [\hat{H}, \hat{Q}_{pq}]]|0\rangle, \tag{3.13}$$

and

$$\left(\underline{\underline{G}}_{SS}\right)_{m,n} = \left(\underline{\underline{G}}_{SS}\right)_{n,m} = -\langle 0^*|[\hat{R}_m, \hat{H}, \hat{R}_n]|0\rangle; \tag{3.14}$$

and $p > q$, $r > s$, $m \neq 0$ and $n \neq 0$. Here

$$[\hat{A}, \hat{B}, \hat{C}] = \tfrac{1}{2}[\hat{A}, [\hat{B}, \hat{C}]] + \tfrac{1}{2}[[\hat{A}, \hat{B}], \hat{C}] \tag{3.15}$$

is the symmetric double commutator, where

$$[\hat{A}, \hat{B}] = \hat{A}\hat{B} - \hat{B}\hat{A} \tag{3.16}$$

is the commutator for three arbitrary linear operators $\hat{A}$, $\hat{B}$ and $\hat{C}$.[50,59]

The search for the stationary point is performed by setting the first derivatives of $q(\underline{\lambda})$ with respect to the elements of the step–length vector ($\{\kappa_{pq}\}$ and $\{S_{n0}\}$) to zero, and then solving for $\{\kappa_{pq}\}$ and $\{S_{n0}\}$, which lead to the following multidimensional Newton–Raphson equation:[50,59]

$$\underline{\lambda} = -\underline{\underline{G}}^{-1}\underline{F}. \tag{3.17}$$

Note that Eq. (30) in Reference, 50 which corresponds to Eq. (3.17) above, is incorrect (for the correct version see Reference 59).

At this point, it is clear that these equations are the same as the ones in quadratically convergent MCSCF using a multidimensional Newton–Raphson approach[29,30] with consideration for biorthogonal states and orbitals and a complex scaled Hamiltonian as was pointed out by Yeager and Mishra.[50] Hence, existing MCSCF codes can be used after adapting them for complex numbers and a modification in the algorithm for the controlled walk on the complex energy hypersurface. This is the same for all standard ab initio methods.[50]

2. Constrained Optimization Algorithm for CMCSCF

A previously developed technique[36] based on Fletcher algorithm[60] for controlling the step–length outside the quadratic region guarantees convergence within a very few iterations for a MCSCF calculations in real space for the lowest energy state of each symmetry. In case of CMCSCF, for the cases where the imaginary part of the step–length vector is usually small compared to its real part, a similar control of just the real part can help expedite the convergence. In this section, first we shall outline the method of step–length control used in MCSCF and then show how to modify it in order to adapt it for CMCSCF.

Following Jørgensen et al.,[36] for MCSCF the control of the step–length ($\underline{\lambda}$) may be described as the optimization of the total energy subject to the constraint

$$\|\underline{\lambda}\| \leq h, \tag{3.18}$$

where h is a pre-defined small positive number ("trust radius"); or in other words, as the optimization of the Lagrangian function,

$$L\left(\underline{\lambda}, \nu\right) = q\left(\underline{\lambda}\right) + \left(\nu/2\right)\left(\underline{\lambda}^{\dagger}\underline{\lambda} - h^2\right), \tag{3.19}$$

where $\nu/2$ is a Lagrange multiplier which is real. This leads to the modified Newton–Raphson equation

$$\underline{\lambda}(\nu) = -\left(\underline{\underline{G}} + \nu\underline{\underline{I}}\right)^{-1}\underline{F}, \tag{3.20}$$

where $\underline{\underline{I}}$ is the identity matrix. The constrained step–length, $\underline{\lambda}(\nu)$, is calculated from

$$\underline{\underline{U}}\,\underline{\ell}(\nu) = \underline{\lambda}(\nu) \tag{3.21}$$

where $\underline{\underline{U}}$ is the unitary matrix that diagonalizes $\underline{\underline{G}}$, i.e.

$$(\underline{\underline{U}}^{-1}\underline{\underline{G}}\,\underline{\underline{U}})_{ij} = \delta_{ij}\, g_j \tag{3.22}$$

with $\{g_j\}$ being the eigenvalues of $\underline{\underline{G}}$, and the elements of $\underline{\ell}$ are obtained from

$$\ell_j(\nu) = -(g_j + \nu)^{-1} f_j, \tag{3.23}$$

where f_j is an element of

$$\underline{f} = \underline{\underline{U}}^{-1}\underline{F}, \tag{3.24}$$

and ν is calculated numerically from

$$\|\underline{\ell}(\nu)\| = \left[\sum_j \ell_j^2(\nu)\right]^{1/2} = h \tag{3.25}$$

(notice that ℓ_j is real in this case) such that the number of negative eigenvalues of the "shifted" Hessian $(\underline{\underline{G}} + \nu\underline{\underline{I}})$ is correct for the state being optimized (i.e., 0 for the ground state of a certain symmetry, 1 for the first excited state of a certain symmetry, etc.). The step–length vector $(\underline{\lambda}^{(k+1)})$ obtained this way using the orbitals and states in the k-th iteration is accepted if $0 < r^{(k)} < 1.5$, where

$$r^{(k)} = (E^{(k+1)} - E^{(k)})/(q^{(k+1)} - E^{(k)}); \tag{3.26}$$

otherwise $\underline{\lambda}^{(k+1)}$ is calculated again using a smaller trust radius, $h^{(k)}$. The ratio $r^{(k)}$ measures the accuracy to which $q(\underline{\lambda}^{(k+1)})$ approximates $E(\underline{\lambda}^{(k+1)})$, i.e. the closer $r^{(k)}$ is to unity, the better the agreement. There are also different schemes[36,60] to choose

the next trust radius ($h^{(k+1)}$) based on how far off $r^{(k)}$ is from unity. This method "guarantees" convergence to the lowest state of certain spin and spatial symmetry.[36,60]

The norm,

$$\|\underline{\lambda}(\nu)\| = \|\underline{\ell}(\nu)\| \tag{3.27}$$

as a function of ν has a structure in case of MCSCF (see Figure 1 in Reference 36), which enables one to employ such a method that constrains the step–length in such a way that it converges to the correct stationary point. However, such structure of $\|\underline{\lambda}(\nu)\|$ is absent in case of CMCSCF as g_j and f_j are complex numbers, but ν must be real in order to avoid incorporation of a complicated complex–root finding subroutine. We calculate ν from

$$\|\underline{l}(\nu)\| = \left[\sum_j l_j^2(\nu)\right]^{1/2} = h, \tag{3.28}$$

where

$$l_j(\nu) = -[\mathrm{Re}(g_j + \nu)]^{-1}\mathrm{Re}(g_j), \tag{3.29}$$

such that the number of negative eigenvalues, $\mathrm{Re}(g_j+\nu)$, of the Hessian are consistent for the state being optimized. This ν is used to calculate $\underline{\ell}(\nu)$ from Eq. (3.23) and then $\underline{\lambda}(\nu)$ from Eq. (3.21). Note that $\underline{\underline{U}}$ is orthogonal in this case. The same test for accepting $\underline{\lambda}^{(k+1)}$ is administered as described above, except for the fact that the ratio is defined here as

$$r^{(k)} = \mathrm{Re}(E^{(k+1)} - E^{(k)})/\mathrm{Re}(q^{(k+1)} - E^{(k)}). \tag{3.30}$$

The rationale for this is the fact that $\|\underline{l}(\nu)\|$ as a function of ν [see Eq. (3.29)] in CMCSCF has similar structure as $\|\underline{\ell}(\nu)\|$ [see Eq. (3.23)] in MCSCF, which makes it easy to find a suitable ν.

C. Results and Discussion

1. Computational Details

While investigating Be^- resonances using complex scaled electron propagator method (single configuration based), Venkatnathan et al.[57] found $14s11p$ basis set to be the best for this case (see Table 1). Hence, we chose to use the same basis set for our calculations.

Be atom has large non-dynamical correlation from considerable mixing of $1s^22p^2$ configuration with the principal $1s^22s^2$ configuration.[32–35] So, for Be^- the choice of $2s2p$ complete active space (CAS) is a reasonable starting point. However, in order to correlate $2s$ and $2p$ properly $2s2p3s3p$ CAS is a better choice for Be^-.

The incoming electron is very loosely bound to the target. We showed[59] that the resonant p electron lies mostly outside the region of the active orbitals. In the current calculation, a single electron was placed in a p orbital outside the CAS, two valence electrons were placed in the CAS and the $1s$ orbital was occupied by two core electrons, such that the overall symmetry was ^2P. The total energies of these Be^- states relative to neutral Be target, $\varepsilon(\eta)$, were used to locate the resonance(s) using the trajectory method. It was found that two of these trajectories show proper cusp behavior indicating resonances. These will be referred as "resonance 1" and "resonance 2". In all the CMCSCF iterations the number of $\mathrm{Re}(g_j)$ (real part of the eigenvalues of the Hessian) values were one and two for resonances 1 and 2, respectively. No resonance was obtained with zero or more than two negative eigenvalues of the Hessian. The final θ–trajectories for these two resonances are shown in Figures 2 and 3, respectively.

In order to compare with complex SCF (CSCF), i.e. SCF using a complex

Table 1. The $14s11p$ basis set for beryllium used in this work. (see References 25,57,61).

s–Type Contractions		p–Type Contractions	
Index	Exponents	Index	Exponents
1	3630.38000000	1	6.84070796
2	532.28000000	2	3.02686193
3	117.79900000	3	1.33931944
4	32.65620000	4	0.59261922
5	10.48010000	5	0.26222089
6	3.66826000	6	0.11602694
7	1.35431000	7	0.05133936
8	0.38905000	8	0.02271653
9	0.15023000	9	0.01005156
10	0.05240600	10	0.00444759
11	0.02600000	11	0.00196796
12	0.01300000		
13	0.00650000		
14	0.00325000		

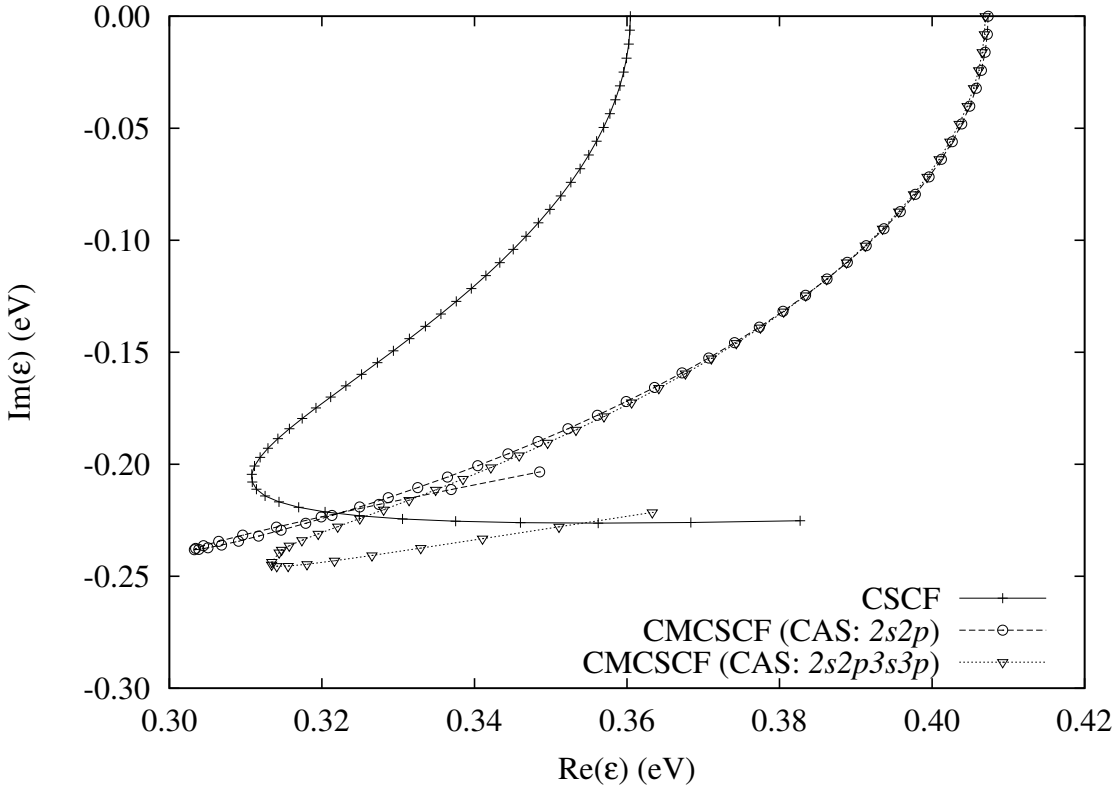

Figure 2. The θ–trajectories for resonance 1 using CSCF, CMCSCF with a $2s2p$ CAS, and CMCSCF with a $2s2p3s3p$ CAS. The values of α (α_o) are 1.005, 0.980 and 0.980, respectively. In each of the trajectories θ started with a value of 0 at the top where $\mathrm{Im}(\varepsilon) = 0$, and incremented linearly in steps of 0.01 radian up to $\theta = 0.500$ radian.

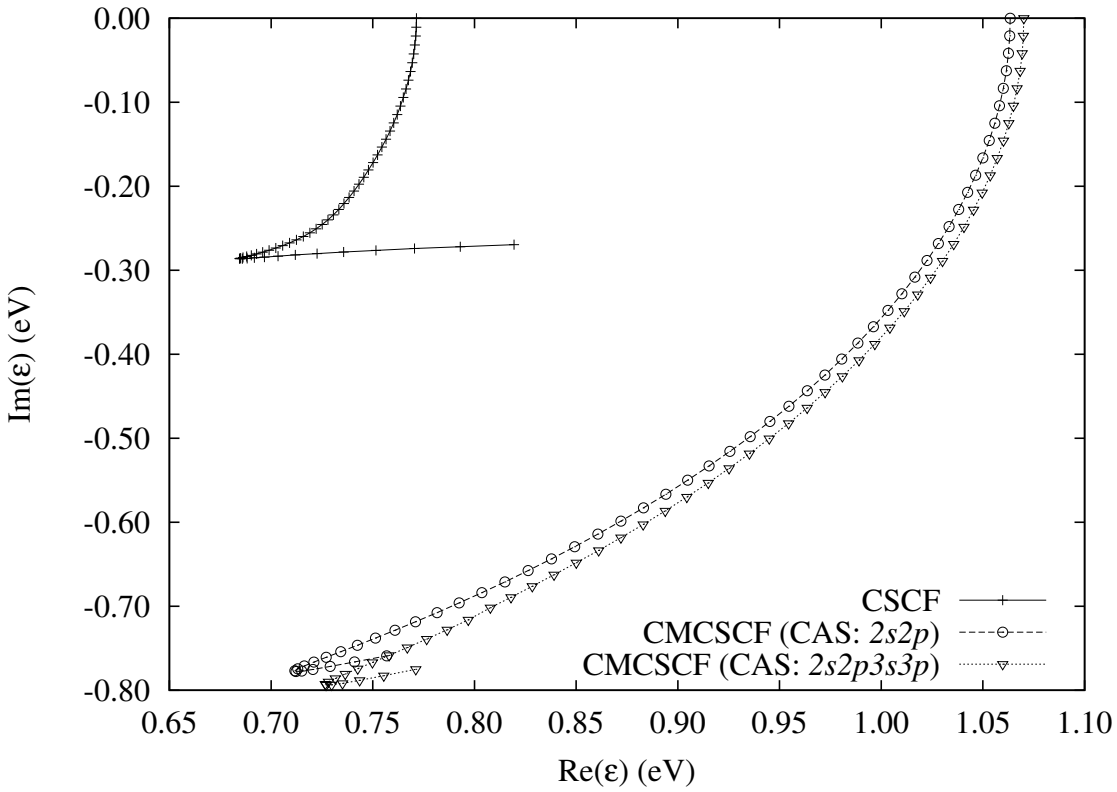

Figure 3. The θ–trajectories for resonance 2 using CSCF, CMCSCF with a $2s2p$ CAS, and CMCSCF with a $2s2p3s3p$ CAS. The values of α (α_o) are 1.020, 0.985 and 0.980, respectively. In each of the trajectories θ started with a value of 0 at the top where $\mathrm{Im}(\varepsilon) = 0$, and incremented linearly in steps of 0.01 radian up to $\theta = 0.550$ radian.

scaled Hamiltonian, we also calculated the total energies using a single determinantal wavefunction using Eqs. (3.6) - (3.17). Resonances from CSCF were obtained for only one and two negative eigenvalues of the Hessian as well, which are shown in Figures 2 and 3 along with the CMCSCF trajectories.

Since the CMCSCF method is new, a few words about its convergence is necessary. We observed that the convergence was achieved with a tolerance of 1.0×10^{-10} a.u. for all the elements of the first derivative vector within ten iterations or less. Table 1 shows the convergence in a typical quadratically convergent CMCSCF calculation. All our calculations were done on a cluster of three 64-core Altix 450 machines with Itanium2 Montecito dual core CPUs. The computer time necessary to complete a CMCSCF calculation is very small (e.g., it took 17.70 seconds of CPU time to complete the calculation in Table 2).

2. Resonance Positions and Widths from CMCSCF

The resonance positions and widths determined from these plots are listed in Table 3. For resonance 1, the resonance positions are found to be 0.31, 0.30 and 0.31 eV for CSCF, CMCSCF with $2s2p$ CAS and CMCSCF with $2s2p3s3p$ CAS, respectively, and the respective widths to be 0.40, 0.48 and 0.49 eV. For resonance 2, the positions are found to be 0.68, 0.71 and 0.73 eV, and the widths 0.58, 1.56 and 1.58, respectively.

We have listed a summary of results obtained by others in Table 4. The positions for resonance 1 in this work are very close to the numbers reported for singles, doubles, and triples complex CI,[68] whereas the results for resonance 2 are close to the positions and widths obtained from static exchange phase shift calculation.[62] However, all of the results by others listed in Table 4 were for only one resonance.

Table 2. Typical convergence of a quadratically convergent CMCSCF calculation with $2s2p3s3p$ CAS for resonance 1. Here $\alpha = 0.980, \theta = 0.410$ radian, and the initial guess of orbitals are the CMCSCF orbitals with $\alpha = 0.980$ and $\theta = 0.405$.

Iteration	Trust Radius	Largest Gradient	$\|\underline{\lambda}\|$	Total Energy
1	0.5	$10^{-2} + 10^{-1}i$	10^{-1}	$-14.60687198 - 0.00901044i$
2	0.5	$10^{-4} + 10^{-3}i$	10^{-2}	$-14.60653248 - 0.00899886i$
3	0.5	$10^{-5} + 10^{-4}i$	10^{-3}	$-14.60653363 - 0.00899915i$
4	0.5	$10^{-7} + 10^{-7}i$	10^{-6}	$-14.60653363 - 0.00899915i$
5	0.5	$10^{-11} + 10^{-11}i$	$< 10^{-10}$	$-14.60653363 - 0.00899915i$

Table 3. ^2P Be^- shape resonance positions and widths from CMCSCF calculation.

Method	Position (eV)	Width (eV)	α_o	θ_o (rad)
Resonance 1				
CSCF	0.31	0.40	1.005	0.375
CMCSCF (CAS: $2s2p$)	0.30	0.48	0.980	0.415
CMCSCF (CAS: $2s2p3s3p$)	0.31	0.49	0.980	0.405
Resonance 2				
CSCF	0.68	0.58	1.020	0.420
CMCSCF (CAS: $2s2p$)	0.71	1.56	0.985	0.490
CMCSCF (CAS: $2s2p3s3p$)	0.73	1.58	0.980	0.495

Table 4. ^2P Be^- shape resonance positions and widths from literature.

Method	Position (eV)	Width (eV)
Static exchange phase shift[62]	0.77	1.61
Static exchange phase shift plus polarizability phase shift[62]	0.20	0.28
Static exchange cross-section[63]	1.20	2.60
Static exchange plus polarizability cross-section[63]	0.16	0.14
ΔSCF with complex $14s16p$ Gaussian basis set[25]	0.70	0.51
ΔSCF with complex $5s14p$ (Slater-type) basis set[9]	0.76	1.11
Singles, doubles, and triples complex CI[64]	0.32	0.30
S matrix pole (X_α)[65,66]	0.10	0.15
Second order dilated electron propagator based on real SCF[67]	0.57	0.99
Bi-orthogonal dilated electron propagator (Basis set $14s11p$):[57]		
Zeroth order	0.62	1.00
Quasiparticle second order	0.61	1.00
Second order	0.48	0.82
Quasiparticle third order	0.54	0.82
OVGF third order	0.54	0.78
Third order	0.53	0.85

3. The Resonance Orbitals

In order to see how an orbital (say, $\tilde{\varphi}_b$), especially the resonant p orbital, obtained from the CSCF and CMCSCF calculations look, we plotted its *radial distributions*, $P_b(r)$, which we define as (see Section 3 of Chapter IV for a detailed discussion on this):

$$P_b(r)dr = N_b^{-1}\, r^2 dr \int_0^{\pi} \sin\theta\, d\theta \int_0^{2\pi} d\phi\, |\tilde{\varphi}_b(r,\theta,\phi)|^2 \tag{3.31}$$

with the choice of

$$N_b = \langle \tilde{\varphi}_b | \tilde{\varphi}_b \rangle \tag{3.32}$$

so that

$$P_b(r) \geq 0\ \forall r \geq 0. \tag{3.33}$$

The plots of $P_b(r)$ for the resonant p orbital as a function of r are shown in Figures 4 and 5 for resonance 1 and resonance 2, respectively. In both the cases, the shape of the plots for the CMCSCF with $2s2p$ and $2s2p3s3p$ CAS choices are almost identical, although they differ quite a bit from that for the CSCF.

In case of resonance 1, the $r_{\rm rms}$ values, where

$$r_{\rm rms}^2 = \int_0^{\infty} r^2 P_b(r) dr, \tag{3.34}$$

for the resonant p are estimated to be 13.96, 23.30 and 23.29 bohrs for CSCF, CMCSCF with $2s2p$ CAS and CMCSCF with $2s2p3s3p$ CAS, respectively. For resonance 2, the respective values are 17.97, 17.73 and 17.72 bohrs.

To see how the resonant p orbitals compare with the orbitals in the CAS, we calculated $r_{\rm rms}$ of the $2s$ and the $2p$ orbitals as well at the CMCSCF stationary points where the resonances were discovered. In case of resonance 1, the $r_{\rm rms}$ values of the $2s$

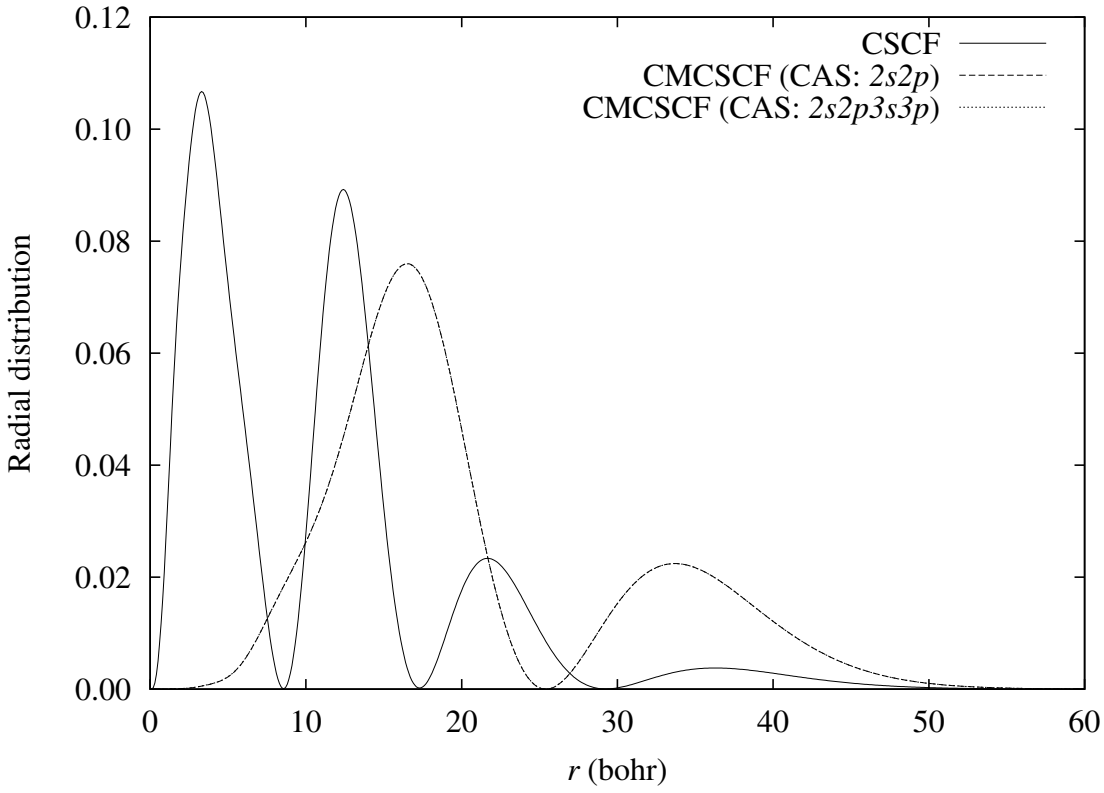

Figure 4. Plot of radial distributions of the resonant p orbital as functions of the radial distance from the nucleus (r) for CSCF, CMCSCF with $2s2p$ CAS and CMCSCF with $2s2p3s3p$ CAS for resonance 1 (The plots for the two CMCSCF cases overlap each other).

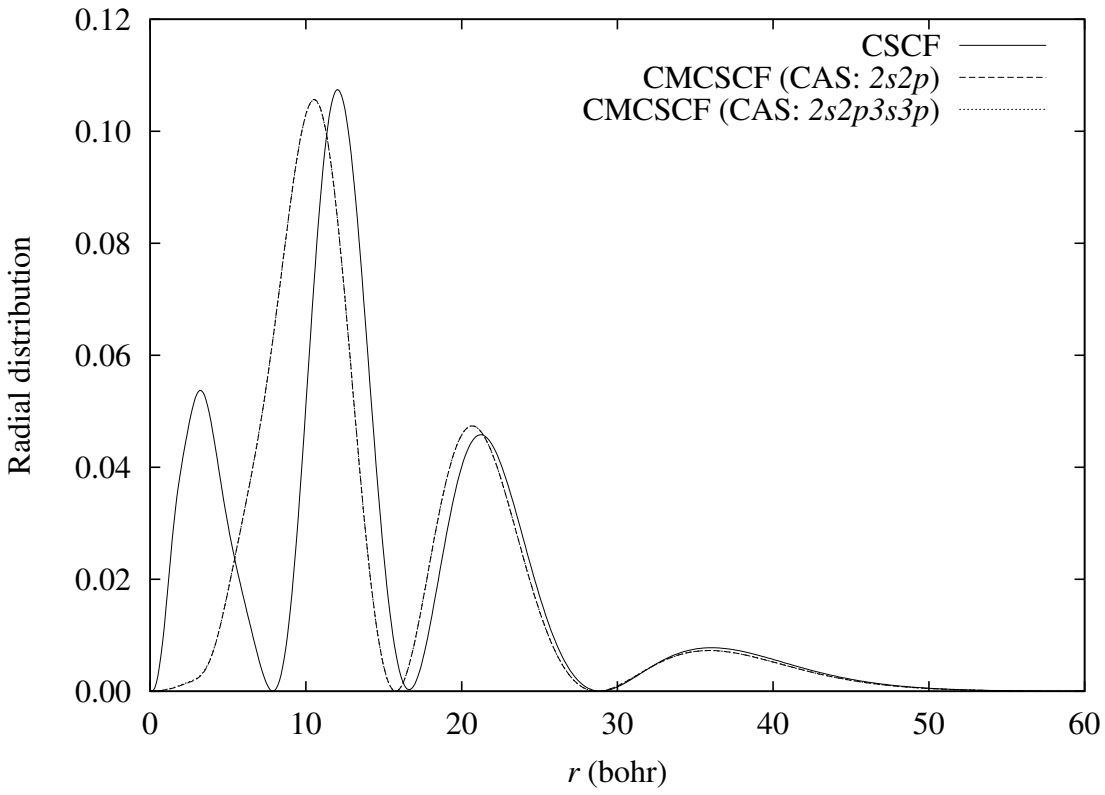

Figure 5. Plot of radial distributions of the resonant p orbital as functions of the radial distance from the nucleus (r) for CSCF, CMCSCF with $2s2p$ CAS and CMCSCF with $2s2p3s3p$ CAS for resonance 2 (The plots for the two CMCSCF cases overlap each other).

and the $2p$ orbitals are 3.00 and 3.22 bohrs for $2s2p$ CAS, and 3.04 and 3.43 bohrs for $2s2p3s3p$ CAS, respectively. In case of resonance 2, the respective values are 3.07 and 3.75 bohrs for $2s2p$ CAS, and 3.11 and 3.93 bohrs for $2s2p3s3p$ CAS. These numbers show that the resonant p orbital lies away from the region of the active orbitals. The r_{rms} values for the $2s$ orbital at the CSCF stationary points at the positions of resonances 1 and 2 are 3.02 and 3.19 bohrs, respectively.

The difference in shapes of both the resonance orbitals and small r_{rms} in case of CSCF for resonance 1 compared to those for CMCSCF are attributable to there being no correlating $2p$ orbital with CSCF. However, this does not affect the resonance energies much although it does affect the resonance width in case of resonance 2.

The shapes of the radial distribution plots for the resonance 2 in the current work (Figure 4) are similar to those in M_1 method[59] except for the fact that the current ones are more spread–out and further out in space due to orbital and state relaxation. However, the plots for resonance 1 are quite different from those seen in case of M_1 method. This is caused by the greater overlap with the valence electrons in the M_1 method than that in the CSCF/ CMCSCF cases because the resonant electron lies further out in the latter.

The changes in the shapes of some of the resonant orbitals and r_{rms} on going from M_1 to the CSCF/ CMCSCF indicates that relaxation effects are important for these resonances. There are also changes going from CSCF to CMCSCF as shown in this work, which demonstrates that non-dynamical correlation also plays an important role.

D. Summary and Conclusions

We have presented a summary of the theory behind quadratically convergent complex multiconfigurational self-consistent field method (CMCSCF) that uses a complex scaled Hamiltonian. The use of complex scaled Hamiltonian enables one to search for the resonances that lie in the continuum part of the Hamiltonian using a bound states method such as multiconfigurational self-consistent field theory (MCSCF). In order to control the walk on the complex energy hypersurface for a CMCSCF calculation far from convergence, a modified constrained optimization algorithm is used.

The continuum ^2P Be^- states are investigated in search for shape resonances. The quadratic convergence of the CMCSCF method, coupled with the use of the modified constraint algorithm, enables convergence with a tolerance of 1.0×10^{-10} for the largest element of the energy gradient within ten iterations or less, starting from a reasonable initial guess. Computational time necessary to obtain resonance positions and widths are modest.

Using CSCF (complex SCF, i.e. CMCSCF in the limit of a single configuration) and CMCSCF, we have shown that there exist two shape resonances of ^2P symmetry for Be^-. This was also shown by our previous calculations. Our best CMCSCF calculation (with the $2s2p3s3p$ CAS) for the resonance positions are 0.31 and 0.73 eV and the respective widths are 0.49 and 1.58 eV for the two resonances.

The radial distribution plots and the $r_{\rm rms}$ values from this work on Be^- shape resonances show that both relaxation and non-dynamical correlation effects are important. This justifies the use of an MCSCF-based method to study resonances.

CHAPTER IV

OBTAINING RESONANCE POSITIONS AND WIDTHS FROM THE M_1 METHOD BASED ON A MULTICONFIGURATIONAL SELF-CONSISTENT FIELD STATE

A. Introduction

In our previous study,[59] we used the multiconfigurational self-consistent field method using a complex scaled Hamiltonian (CMCSCF) to investigate resonances. However, in order to use this direct CMCSCF method to study a resonance, several of the excited states of the ionic species must be investigated in separate calculations first. In this chapter we develop M_1 method based on the multiconfigurational spin–tensor electron propagator (MCSTEP) method. This method allows us to test several potential resonance roots from a single calculation.

Resonance energy is traditionally reported as the total energy of the resonance state relative to the total energy of the scattering target. In direct CMCSCF, first the total energy of the resonant state was calculated and then the resonance energy was calculated by subtracting the total energy of the neutral target, which, in terms of the computational chemistry, may incorporate some "subtraction error". The possibility of this error is not present in the M_1 method since it calculates the resonance energy directly.

In the next section we present the theoretical framework of the M_1 method. After that, we present our computational results. At the end we summarize and conclude our discussion.

B. The M_1 Matrix and the Calculation of Resonance Energy

Multiconfigurational spin tensor electron propagator (MCSTEP) is a very powerful tool for calculating accurate ionization potentials (IPs) and electron affinities (EAs) accurately for correlated systems including open shell atoms and molecules that have non-dynamical correlation in their initial (or reference) states.[33–35,69–75] The MCSTEP IPs/EAs are obtained by solving the following eigenvalue equation[33]

$$\underline{\underline{M}}\,\underline{X}_f = \omega_f\,\underline{\underline{N}}\,\underline{X}_f. \tag{4.1}$$

where

$$\begin{aligned}(\underline{\underline{M}})_{rp} &= \sum_{\Gamma}(-1)^{S_0-\Gamma-S_f-\gamma_r}W(\gamma_r\gamma_p S_0 S_0;\Gamma S_f)\\ &\quad\times(2\Gamma+1)^{1/2}\langle NS_0||\{h_r^\dagger(\bar{\gamma}_r),\hat{\mathcal{H}},h_p(\gamma_p)\}^\Gamma||NS_0\rangle,\end{aligned} \tag{4.2}$$

$$\begin{aligned}(\underline{\underline{N}})_{rp} &= \sum_{\Gamma}(-1)^{S_0-\Gamma-S_f-\gamma_r}W(\gamma_r\gamma_p S_0 S_0;\Gamma S_f)\\ &\quad\times(2\Gamma+1)^{1/2}\langle NS_0||\{h_r^\dagger(\bar{\gamma}_r),h_p(\gamma_p)\}^\Gamma||NS_0\rangle,\end{aligned} \tag{4.3}$$

ω_f is an IP or EA from the N-electron initial tensor state $|NS_0\rangle\rangle$ with spin S_0 to the $(N\pm1)$-electron final ion tensor state $|(N\pm1)S_f\rangle\rangle$ with spin S_f, W is the usual Racah coefficient, $\hat{\mathcal{H}}$ is the Hamiltonian (real and unscaled), and $h_p(\gamma_p)$ and $h_r^\dagger(\bar{\gamma}_r)$ are the tensor operator versions of the operator manifold with ranks γ_p and γ_r, respectively. Here

$$\{\hat{A},\hat{B},\hat{C}\} = \tfrac{1}{2}\{\hat{A},[\hat{B},\hat{C}]\} + \tfrac{1}{2}\{[\hat{A},\hat{B}],\hat{C}\} \tag{4.4}$$

is the symmetric double anticommutator with

$$\{\hat{A}, \hat{B}\} = \hat{A}\hat{B} + \hat{B}\hat{A} \tag{4.5}$$

as the anticommutator for the arbitrary linear operators, $\hat{A}$, $\hat{B}$ and $\hat{C}$.

$\underline{\underline{M}}$ has five non-zero blocks and each one involves a combination of tensor operators. The first block, $\underline{\underline{M_1}}$, which involves simple electron creation and annihilation operators, is the most important one for principal ionization potentials and simple electron attachment energies. The first block of $\underline{\underline{N}}$ is the identity matrix.

In this work, we define $\underline{\underline{M_1}}$ for a closed system in a similar way as in MCSTEP except that its initial state is a CMCSCF state ($|\tilde{0}\rangle$), the Hamiltonian, $\hat{\mathcal{H}}$ is complex scaled to $\hat{H}$ by means of complex scaling the electronic coordinates ($\mathbf{r}$) as $\eta\mathbf{r}$ where $\eta = \alpha \exp(i\theta)$ ($\alpha \in \mathbb{R};\ \theta \in \mathbb{R}$), and the creation and annihilation operators correspond to a biorthogonal set of spin orbitals $\{\varphi_b\, \sigma\}$:

$$(\underline{\underline{M_1}})_{cd} = \langle \tilde{0}^* | \{a^T_{c\sigma}, \hat{H}, a_{d\sigma'}\} | \tilde{0} \rangle, \tag{4.6}$$

Notice the use of $a^T_{c\sigma}$ (creation) and $a_{d\sigma'}$ (annihilation) operators, which correspond to the spin orbitals $\varphi_c\, \sigma$ and $\varphi_d\, \sigma'$, respectively. The spin functions σ and σ' are either α or β, and φ_c and φ_d are spatial orbitals. We will use the same symbol φ for spatial and spin orbitals, but reserve the letters in the beginning of the alphabet (e.g. b, c, d, e, etc.) to label the spatial orbitals, and those at the end (e.g. p, q, r, s, etc.) for the spin orbitals in order to avoid confusion.

Upon writing Eq. (4.6) explicitly as

$$(\underline{\underline{M_1}})_{cd} = -h_{cd}\delta_{\sigma\sigma'} + \sum_{b,e} V_{bcde}\langle\tilde{0}^*|a^T_{b\sigma}a_{e\sigma'}|\tilde{0}\rangle - \sum_{b,e,\sigma} V_{cbde}\langle\tilde{0}^*|a^T_{b\sigma}a_{e\sigma}|\tilde{0}\rangle, \tag{4.7}$$

one can see that $\underline{\underline{M_1}}$ has the same form as the negative of the Fock matrix (complex) if $|\tilde{0}\rangle$ is a single determinantal wavefunction; and, hence, in that case its eigenvalues are the IPs/EAs at the Koopmans' theory level. With a better $|\tilde{0}\rangle$, i.e. a larger complete active space (CAS) choice, the eigenvalues are much better approximations to the ionization and attachment energies.

IPs/EAs are generally reported as positive numbers, and in that spirit we define an IP or an EA as

$$\varepsilon = [\mathrm{sgn}(\mathrm{Re}(\omega_f))]\omega_f. \tag{4.8}$$

Since $\varepsilon(\eta)$ is related to the total energy, $E_c^{N\pm1}(\eta)$, of an $(N \pm 1)$-electron resonance state originated from the scattering of an electron off an N-electron bound state target with energy E_b^N (independent of η) as

$$E_c^{N\pm1}(\eta) = E_0^N \mp \varepsilon(\eta), \tag{4.9}$$

we can use Eqs. (2.22) and (2.23) to calculate resonance energy, $\varepsilon(\eta_o)$, using the trajectory method.

C. Results and Discussion

1. Computational Details

In this study we investigated ^2P Be^- shape resonances using M_1 method. The initial state for $\underline{\underline{M_1}}$ was obtained by performing CMCSCF calculations on neutral beryllium atom. Be has a fairly large amount of non-dynamical correlation since the $1s^22p^2$ configuration has considerable mixing ($\sim 10\%$ of $|\tilde{0}\rangle$ for $\eta = 1$) with the principal $1s^22s^2$ configuration.[32,34,35] So both the configurations need to be included non-perturbatively for accurate IP and EA calculations. It was shown[32,34,35] that for very accurate IPs, EAs and excitation energies of Be, a $2s2p3s3p3d$ CAS is necessary. Based on these observations, five different CASs, viz. $2s2p$, $2s2p3s$, $2s2p3p$, $2s2p3s3p$ and $2s2p3s3p3d$, with two electrons were chosen for the CMCSCF calculations. In addition to that, a CMCSCF calculation was done based on a single determinantal wavefunction, thus performing bi-variational SCF (CSCF). Except for the choice of $2s2p$ CAS, all of the active space choices include some dynamical correlation effects, although they are not adequate for approximating all the dynamical correlation.

Venkatnathan et al.[57] performed an extensive basis set study for the same resonance using single configuration based dilated electron propagator (EP) method, and found the $14s11p$ basis set to be the best for this resonance (see Table 1). Hence, we used this basis set for *all* the CSCF/CMCSCF calculations except for the one involving $2s2p3s3p3d$ CAS. The basis set chosen for the calculation with $2s2p3s3p3d$ CAS involves the same fourteen s and eleven p functions as in $14s11p$ basis set mentioned above plus three uncontracted d functions with exponents 0.3480000, 0.1803000 and 0.0934140. The first two of these exponents are the same as for the d functions in Dunning's cc-pVTZ basis set,[76] and the third was added to the first two in a geomet-

ric progression with a view to account for the diffuse nature of the resonances. No d function enters the MCSCF/CMCSCF or M_1 equations unless at least one of the d orbitals is in the CAS.

All the calculations were performed on a cluster of three 64-core Altix 450 machines with Itanium2 Montecito dual core CPUs. Starting from reasonable guesses of initial orbitals, the convergence of the CMCSCF calculation with a tolerance of 1.0×10^{-10} a.u. for the energy gradient was achieved within ten iterations or less for all the cases. The CPU time to converge to the correct CMCSCF stationary point for each η and each CAS choice was found to be trivial (less than 30 seconds, in general).

The α–trajectories of the four lowest p-type EAs, viz. ε_1, ε_2, ε_3 and ε_4 [$\varepsilon_1(\eta = 1) < \varepsilon_2(\eta = 1) < \varepsilon_3(\eta = 1) < \varepsilon_4(\eta = 1)$], obtained from diagonalizing $\underline{\underline{M_1}}$ based on a CSCF initial state, were plotted (Figure 6) in order to see which give rise to some stability as α was changed holding θ constant at a big enough value (= 0.55 radian). It is clear that ε_2 and ε_3 show some hint of stability at around $\alpha = 0.70$ as well as $\alpha = 0.80$, and so they are the potential candidates for ^2P Be^- shape resonances. However the other two do not show any such stability. The outcome was found to be similar (although the stability of ε_2 and ε_3 were at different α values) if CMCSCF with different CAS choices was used instead.

Next, ε_2 and ε_3 were calculated for a series of η values using CSCF as well as CMCSCF with different CAS choices, and the resonance energy was obtained using the trajectory method. Using the optimum values of α, the final θ–trajectories were plotted in Figures 7 and 8, respectively, and the resonance positions and widths were determined from these. The results are listed in Table 5.

Although the loops/cusps clearly indicate the location of the resonance in Figure 8, the "slowing down" of the points is not very clear in Figure 7. Nevertheless, the clear indication of a change in direction of the curves may be taken as an indication

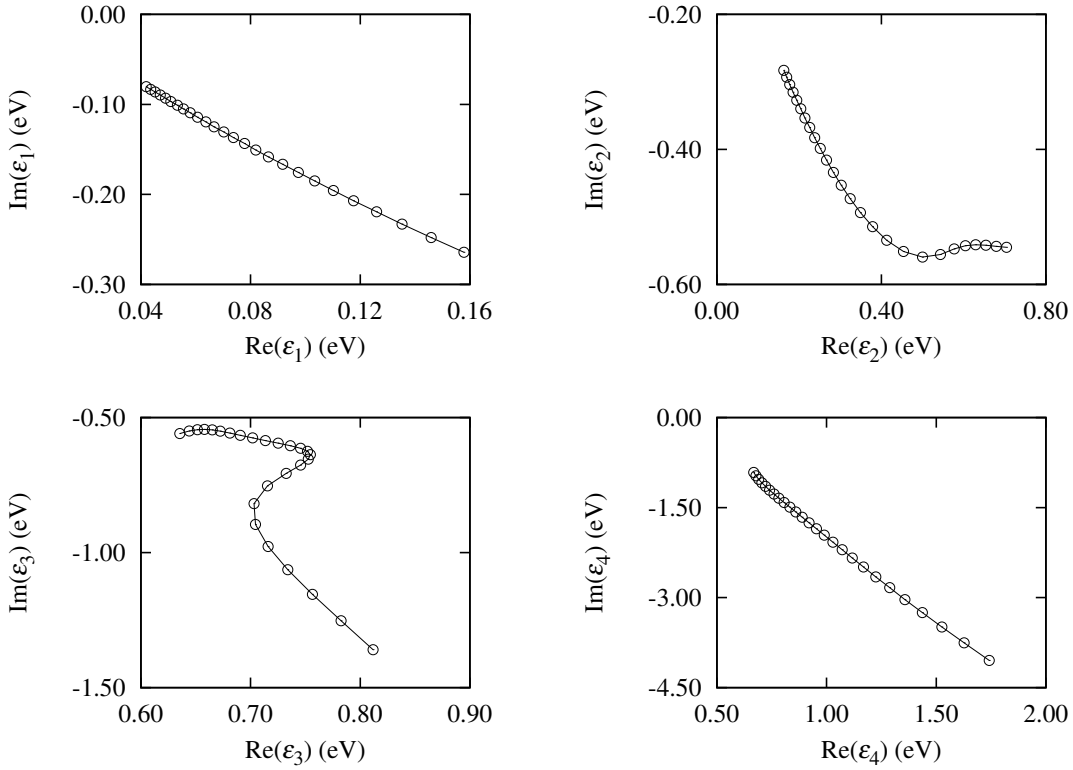

Figure 6. The α–trajectories of the lowest four p-type EAs (ε_1, ε_2, ε_3 and ε_4) obtained from $\underline{\underline{M_1}}$ based on an optimized CSCF state of Be at $\theta = 0.55$ radian. In each of the trajectories, α starts with a value of 0.60 at the right bottom end and incremented linearly in steps of 0.02 up to $\alpha = 1.10$.

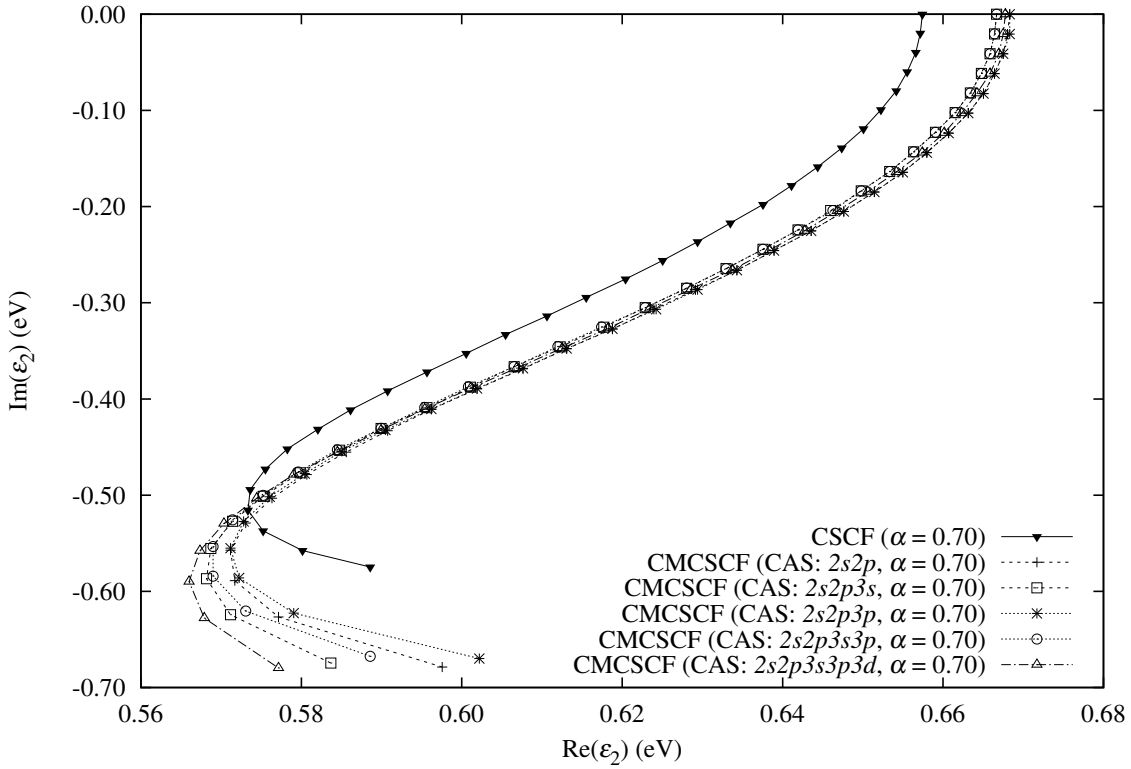

Figure 7. The final θ–trajectories of ε_2 using different initial states (CSCF/ CMC-SCF) for $\underline{\underline{M_1}}$. The trajectories start at the top, where $\mathrm{Im}(\varepsilon_2) = 0$, with $\theta = 0$ and incremented linearly in steps of 0.02 radian up to $\theta = 0.58$ radian.

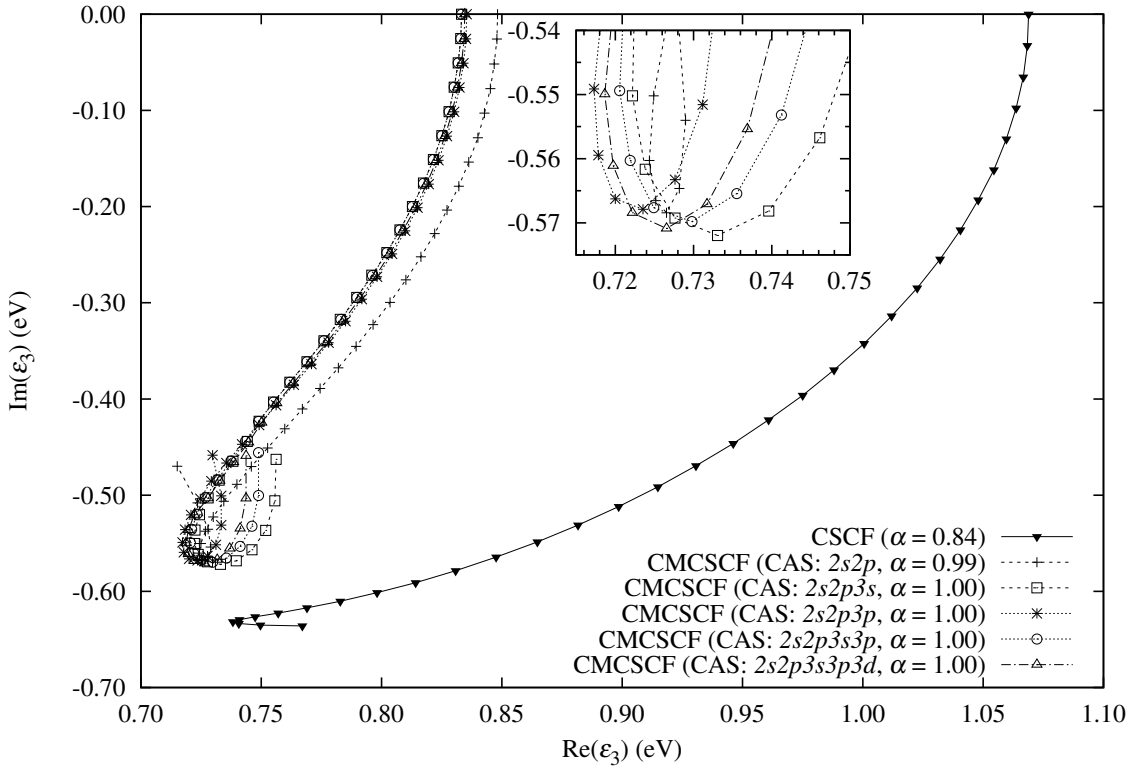

Figure 8. The final θ–trajectories of ε_3 using different initial states (CSCF/ CMC-SCF) for $\underline{\underline{M_1}}$. The trajectories start at the top, where $\mathrm{Im}(\varepsilon_2) = 0$, with $\theta = 0$ and incremented linearly in steps of 0.02 radian up to $\theta = 0.66$ radian.

Table 5. ^2P Be^- shape resonance positions and widths for the resonances 1 and 2 using the M_1 method.

Method	Position (eV)	Width (eV)	α_o	θ_o (radian)
Resonance 1:				
CSCF	0.57	1.01	0.70	0.54
CMCSCF (CAS: $2s2p$)	0.57	1.15	0.70	0.54
CMCSCF (CAS: $2s2p3s$)	0.57	1.16	0.70	0.54
CMCSCF (CAS: $2s2p3p$)	0.57	1.13	0.70	0.53
CMCSCF (CAS: $2s2p3s3p$)	0.57	1.15	0.70	0.53
CMCSCF (CAS: $2s2p3s3p3d$)	0.57	1.19	0.70	0.54
Resonance 2:				
CSCF	0.74	1.26	0.84	0.61
CMCSCF (CAS: $2s2p$)	0.73	1.14	0.99	0.56
CMCSCF (CAS: $2s2p3s$)	0.72	1.11	1.00	0.50
CMCSCF (CAS: $2s2p3p$)	0.72	1.13	1.00	0.51
CMCSCF (CAS: $2s2p3s3p$)	0.72	1.10	1.00	0.50
CMCSCF (CAS: $2s2p3s3p3d$)	0.72	1.12	1.00	0.50

of stabilization in the latter.[11] Notice that the plots in Figure 7 closely resemble those obtained by Mishra and coworkers[11,16,57] using single configuration–based dilated EP method. However, they did not see anything that resembles the plots in Figure 8. This may be because they did not investigate the other poles of the EP beyond $\theta = 0.58$ radian.

2. Positions and Widths of the Resonances

For ^2P Be^- shape resonance corresponding to ε_2 ("resonance 1"), the positions and the widths of the resonance were found to be 0.57 eV and 1.01 eV, 0.57 eV and 1.15 eV, 0.57 eV and 1.16 eV, 0.57 eV and 1.13 eV, 0.57 eV and 1.15 eV, and 0.57 eV and 1.19 eV using the optimized states from CSCF, CMCSCF with a $2s2p$ CAS, CMCSCF with a $2s2p3s$ CAS, CMCSCF with a $2s2p3p$ CAS, CMCSCF with a $2s2p3s3p$ CAS and CMCSCF with a $2s2p3s3p3d$ CAS as the initial state for $\underline{\underline{M_1}}$, respectively (see Table 5). The respective numbers for the resonance corresponding to ε_3 ("resonance 2") were found to be 0.74 eV and 1.26 eV, 0.73 eV and 1.14 eV, 0.72 eV and 1.11 eV, 0.72 eV and 1.13 eV, 0.72 eV and 1.10 eV, and 0.72 eV and 1.12 eV (see Table 5).

For resonance 1, the positions remain the same but the widths differ by a maximum of 18% on going from CSCF to CMCSCF initial states; whereas for resonance 2, the positions and widths differ by a maximum of 2% and 13% on going from CSCF to CMCSCF initial states, respectively.

Results from important previous studies, are listed in Table 4 for comparison. The resonance positions (E_r) and widths (Γ) that we obtained for resonance 1, are very similar to those obtained from the EP calculations by Donnelly and Simons ($E_r = 0.57$ eV and $\Gamma = 0.99$ eV for second order EP)[67] and Venkatnathan et al.

($E_r = 0.48$ eV and $\Gamma = 0.82$ eV using second order EP; $E_r = 0.53$ eV and $\Gamma = 0.85$ eV using third order EP; $E_r = 0.54$ eV and $\Gamma = 0.82$ eV using quasiparticle third order EP; and $E_r = 0.54$ eV and $\Gamma = 0.78$ eV using third order OVGF).[16] On the other hand, the resonance position and width from the ΔSCF calculations using complex $5s14p$ (Slater-type) basis set ($E_r = 0.76$ eV and $\Gamma = 1.11$ eV)[25] as well as from static exchange phase shift calculation ($E_r = 0.77$ eV and $\Gamma = 1.62$ eV)[62] are similar to our results for resonance 2, although the width for the static exchange phase shift calculation is considerably larger than our results. The position obtained from another ΔSCF calculation using a complex $14s16p$ Gaussian basis set ($E_r = 0.77$ eV) is also similar to our result, although the width is smaller ($\Gamma = 0.51$ eV).[9]

The similarity between the numbers obtained from the EP methods above and the M_1 method are not very surprising, because the matrix, $\underline{\underline{M_1}}$ is the first of the five blocks of $\underline{\underline{M}}$ defined in multiconfigurational spin-tensor electron propagator (MCSTEP), another Green's function based method as the former (see Reference 30) to determine ionization potentials and electron affinities. The zeroth order dilated EP is the same as M_1 method when the initial state for $\underline{\underline{M_1}}$ is a CSCF state.

The positions and widths obtained from this study are high compared to the complex configuration interaction (CI) results ($E_r = 0.32$ eV, $\Gamma = 0.30$ eV).[64] This may be due to the fact that the orbitals considered in the M_1 method are not relaxed because the orbitals are obtained from the neutral Be. We also note that the CI calculations did not include any effect of quadruple excitations. It is well-known that these need to be included (e.g. by a Davidson correction[77]) for accurate CI energies and properties. However, our previous study[59] show that if the relaxation effects are taken into account (i.e. if the Be^- orbitals are considered), the numbers are in excellent agreement with the complex CI results. We also want to stress that to obtain accurate resonance energy all the blocks of the M matrix defined in MCSTEP[33] must

be included in the calculation.

Looking at the numbers in Table 4, it appears that the wide ranges of values for position and width in the literature are indicative of the two close lying resonances as revealed in the current work (resonances 1 and 2). Despite the fact that ^2P Be^- shape resonance has always been considered to be the testing ground for new methods of studying scattering resonances, unfortunately, there are to our knowledge, no experimental data to compare with our results.

3. Comparison of the Resonance Orbitals

In order to visualize how the orbitals $\{\varphi_b\}$ look, especially the resonant p orbitals, we calculated their *radial distributions*, $P_b(r)$, which we define as

$$P_b(r)dr = N_b^{-1}\, r^2 dr \int_0^{\pi}\int_0^{2\pi} |\bar{\varphi}_b(r,\theta,\phi)|^2 \sin\theta\, d\theta\, d\phi, \tag{4.10}$$

where

$$\bar{\varphi}_b = \sum_c (\underline{\underline{\Omega}}^T)_{bc}\, \tilde{\varphi}_c \tag{4.11}$$

with $\{\tilde{\varphi}_c\}$ being the CSCF/MCSCF orbitals and $\underline{\underline{\Omega}}$ a matrix that contains the biorthonormalized eigenvectors of $\underline{\underline{M_1}}$ as its columns, and

$$N_b = \langle \bar{\varphi}_b | \bar{\varphi}_b \rangle \tag{4.12}$$

so that

$$P_b(r) \geq 0 \;\forall r \geq 0. \tag{4.13}$$

Although $(\bar{\varphi}_b)^2$, instead of $|\bar{\varphi}_b|^2 = \bar{\varphi}_b^* \bar{\varphi}_b$, in Eq. (4.10) along with

$$N_b = \langle \bar{\varphi}_b^* | \bar{\varphi}_b \rangle \tag{4.14}$$

may seem to be a more reasonable choice because of the biorthogonality of the orbitals, the former causes $P_b(r)$ to be complex, thus making it hard to interpret $P_b(r)$ graphically. This prompted us to use the latter for a more *realistic* $P_b(r)$. Another reason was to be able to compare our plots with those in the literature (e.g., Reference 16). Also notice that $P_b(r)$ is not a *probability distribution* (since the orbitals are complex biorthogonal), although they are related. Caution must be taken in interpreting $P_b(r)$ [as defined in Eq. (4.10)] vs. r plots of the orbitals obtained from the calculations using a complex scaled ($\theta \neq 0$) Hamiltonian, which should not be expected to show the same nodal behavior as the ones obtained from a calculation that uses an unscaled Hamiltonian because of their different orthogonality properties. However, the function,

$$P'_b(r)dr = (N'_b)^{-1} \, r^2 dr \int_0^{\pi} \int_0^{2\pi} [\mathrm{Re}(\bar{\varphi}_b)]^2 \sin\theta \, d\theta \, d\phi, \tag{4.15}$$

where

$$N'_b = \langle \mathrm{Re}(\bar{\varphi}_b) | \mathrm{Re}(\bar{\varphi}_b) \rangle, \tag{4.16}$$

shows similar nodal behavior as the radial density of the real orbitals and is often found to be very useful in identifying the orbitals. Other possible choices for the radial distribution include using $\mathrm{Re}(\bar{\varphi}_b{}^2)$ and $|\mathrm{Re}(\bar{\varphi}_b{}^2)|$.

To demonstrate the differences, we plotted the four choices for the density distribution described above, viz. using $|\bar{\varphi}_b|^2$ [Eq. (4.10)], $[\mathrm{Re}(\bar{\varphi}_b)]^2$ [Eq. (4.15)],

$\mathrm{Re}(\bar{\varphi}_b{}^2)$ and $|\mathrm{Re}(\bar{\varphi}_b{}^2)|$ with appropriate normalizations to unity for the $2s$ orbital at the CSCF stationary point with $\eta = \eta_o$ that uncovered resonance 1 (Figure 9). The plots indicate that first two choices give very good description of the orbital (although the first one does not show proper node structure but does allow for comparison with the results of others, e.g. Reference 16). The third gives rise to negative values at some r which makes it unacceptable. Although the fourth fixes the problem with negative values shown by the third, it gives rise to spurious nodes, and moreover does not have a smooth shape.

The radial distributions of the resonant p orbitals [$P_{\mathrm{res1}}(r)$ and $P'_{\mathrm{res1}}(r)$ for resonance 1, and $P_{\mathrm{res2}}(r)$ and $P'_{\mathrm{res2}}(r)$ for resonance 2] are plotted in Figure 10 for CSCF and CMCSCF with the smallest ($2s2p$) and the largest ($2s2p3s3p3d$) CAS choices. The root-mean-squared (r.m.s.) values of r, i.e. r_{rms} (r'_{rms} in parentheses), where

$$(r_{\mathrm{rms}})^2 = \int_0^\infty r^2 P_b(r) dr \tag{4.17}$$

and

$$(r'_{\mathrm{rms}})^2 = \int_0^\infty r^2 P'_b(r) dr, \tag{4.18}$$

for the resonant p orbital were found to be 18.08 (18.41), 18.66 (19.48) and 18.58 (19.53) bohrs in case of resonance 1, and 10.53 (9.20), 10.25 (9.95) and 12.09 (12.13) bohrs in case of resonance 2 for the calculations involving the optimized states from CSCF, CMCSCF with $2s2p$ CAS, and CMCSCF with $2s2p3s3p3d$ CAS as the initial states for $\underline{\underline{M_1}}$, respectively.

Figure 10 shows that on going from CSCF to CMCSCF, the resonant orbitals become more relaxed and the shoulders become pronounced. However, the shapes of the plots hardly change from the smallest to the largest CAS, which is a typical scenario for an orbital outside the active space. This prompted us to conclude that

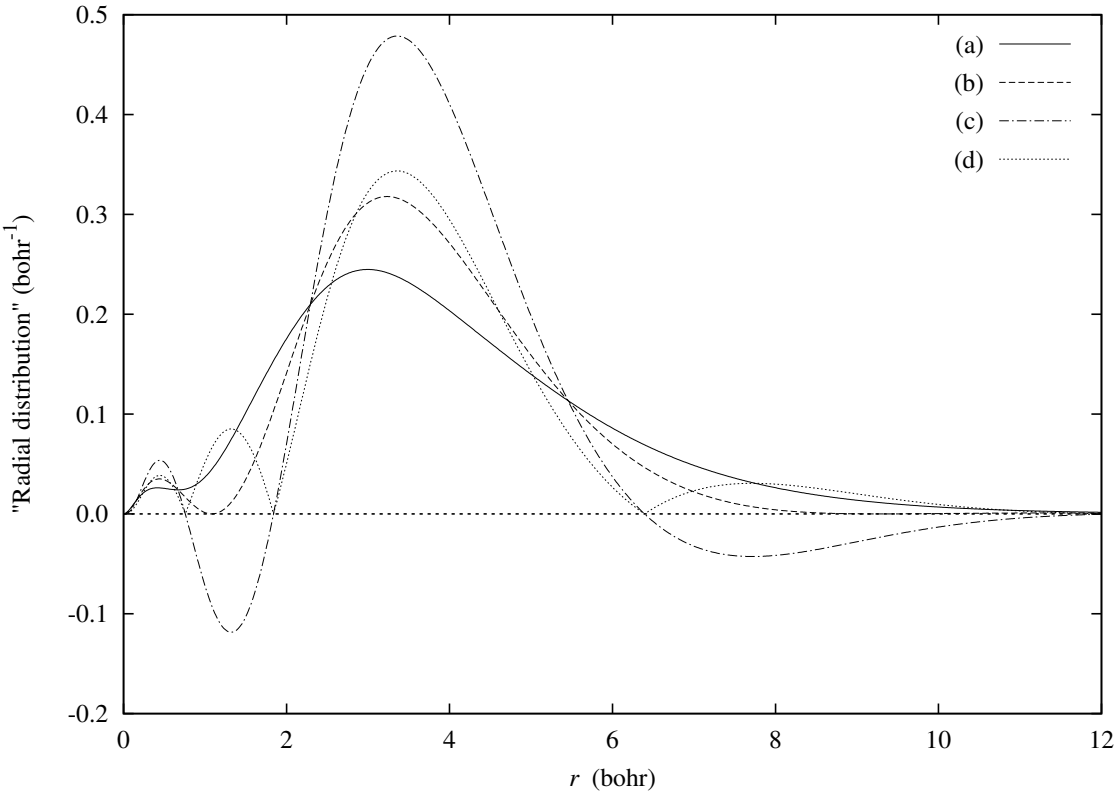

Figure 9. The plots of the "radial distributions" of the $2s$ orbital at the CSCF stationary point with $\eta = \eta_o$ that revealed resonance 1 as functions of r with a view to find the best definition of the radial distribution (one that describes an orbital best). The possible choices are $[r^2 \int_0^{\pi} \sin\theta \, d\theta \int_0^{2\pi} d\phi \, f(r,\theta,\phi)]/[\int_0^{\infty} r^2 dr \int_0^{\pi} \sin\theta \, d\theta \int_0^{2\pi} d\phi \, f(r,\theta,\phi)]$ with f as (a) $|\bar{\varphi}_{2s}|^2$, (b) $[\mathrm{Re}(\bar{\varphi}_{2s})]^2$, (c) $\mathrm{Re}(\bar{\varphi}_{2s}{}^2)$ and (d) $|\mathrm{Re}(\bar{\varphi}_{2s}{}^2)|$.

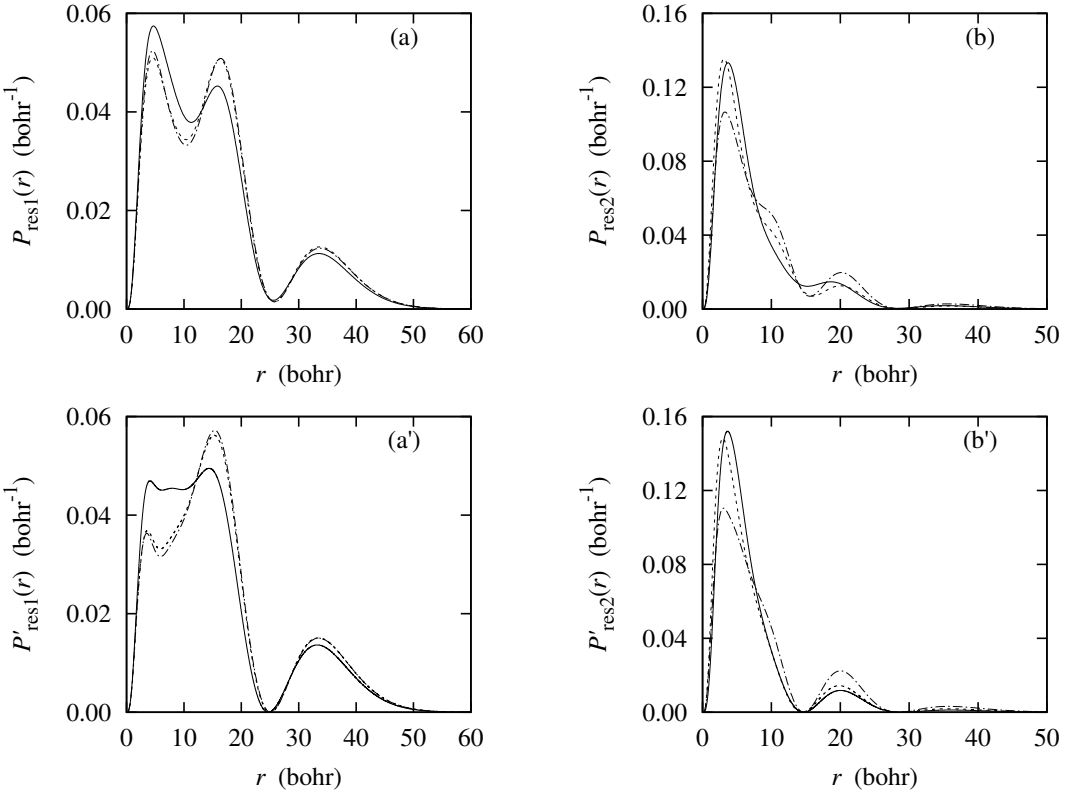

Figure 10. The plots of radial distributions of the resonant p orbital as a function of r in case of resonance 1 (a and a$'$) and resonance 2 (b and b$'$) for CSCF (———), CMCSCF with $2s2p$ CAS (- - - - -) and CMCSCF with $2s2p3s3p3d$ CAS ($-\cdot-\cdot-$) .

both the resonant orbitals from the M_1 method lie outside the space of the active orbitals. This explains why the introduction of a larger CAS does not change the position and the width of the resonances significantly. In order to verify this, we plotted the radial distributions of the correlating $2s$, $P_{2s}(r)$ and $P'_{2s}(r)$, and $2p$ orbitals, $P_{2p}(r)$ and $P'_{2p}(r)$, in Figures 11 and 12, respectively.

The plots in Figures 11 and 12 are based on the orbitals obtained by transforming [see Eq. (4.11)] the CSCF/ CMCSCF orbitals with the eigenvectors of the "partitioned" $\underline{\underline{M_1}}$ where the elements corresponding to occupied–partially occupied, occupied–unoccupied and partially occupied–unoccupied spaces are set to zero. This makes it easy to identify the correlating orbitals (and these are the appropriate[35] orbitals for the converged CMCSCF state). Notice also that in case of SCF, those elements are automatically zero and $\{\bar{\varphi}_b\}$ are the canonical Hartree-Fock orbitals.

For the rotations (η_o) that revealed resonance 1, the $r_{\rm rms}$ ($r'_{\rm rms}$) values of the $2s$ orbital at the CMCSCF stationary points with $2s2p$ and $2s2p3s3p3d$ CAS choices were found to be 4.35 (3.94) and 4.43 (4.01) bohrs, respectively, whereas the respective values for the $2p$ orbital are 4.94 (4.04) and 4.35 (3.95) bohrs. The respective values for the rotation (η_o) that revealed resonance 2 are 3.12 (2.83) and 3.05 (2.78) bohrs for the $2s$ orbital, and 3.23 (3.89) and 3.12 (2.83) bohrs for the $2p$ orbital. For the η_o corresponding to uncovering of resonances 1 and 2, the $r_{\rm rms}$ ($r'_{\rm rms}$) value of the $2s$ orbital at the CSCF stationary points were found to be 4.42 (4.02) and 3.87 (3.46) bohrs, respectively.

Figures 10–12 and $r_{\rm rms}$ ($r'_{\rm rms}$) values clearly indicate that the resonant orbitals lie mostly outside the region of the active orbitals.

In order to see if the two resonances actually indicate a single one, we also plotted (Figure 13) the radial distributions, $P_{\pm}(r)$ and $P'_{\pm}(r)$ [with proper normalization

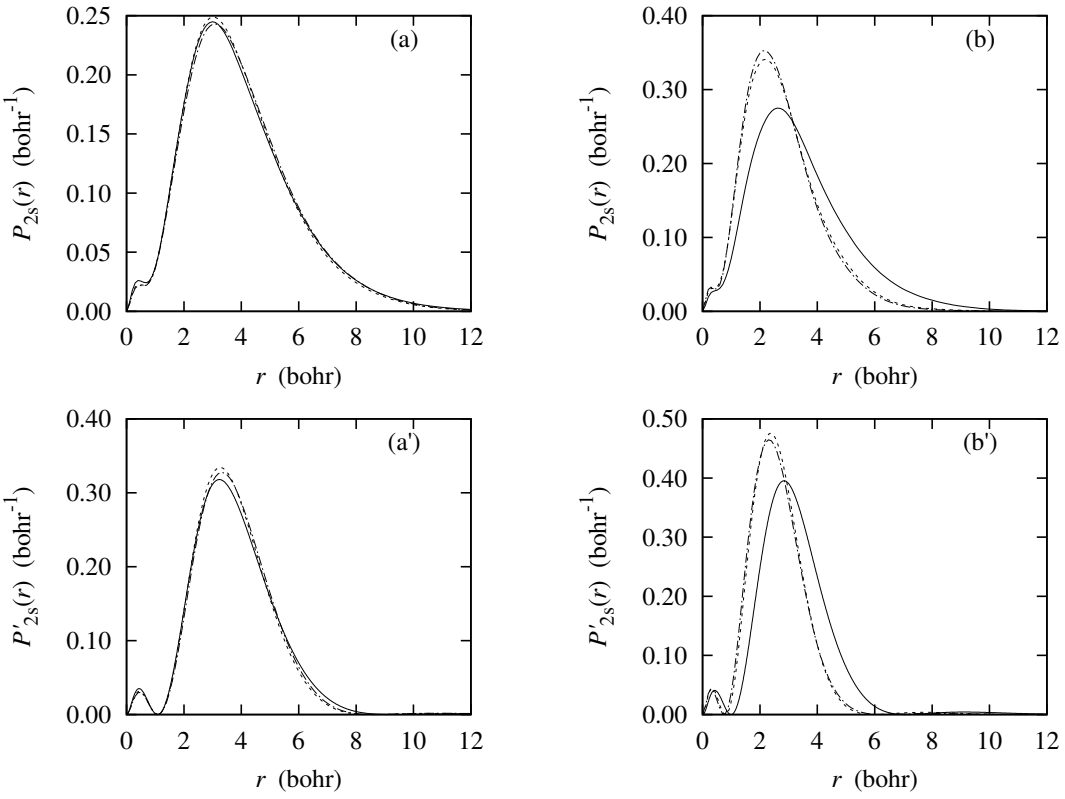

Figure 11. The plots of radial distributions of the $2s$ orbital as a function of r at the CSCF (———), the CMCSCF with $2s2p$ CAS (- - - - -) and the CMCSCF with $2s2p3s3p3d$ CAS ($-\cdot-\cdot-$) stationary points for $\eta = \eta_o$ that revealed resonance 1 (a and a′) and resonance 2 (b and b′) .

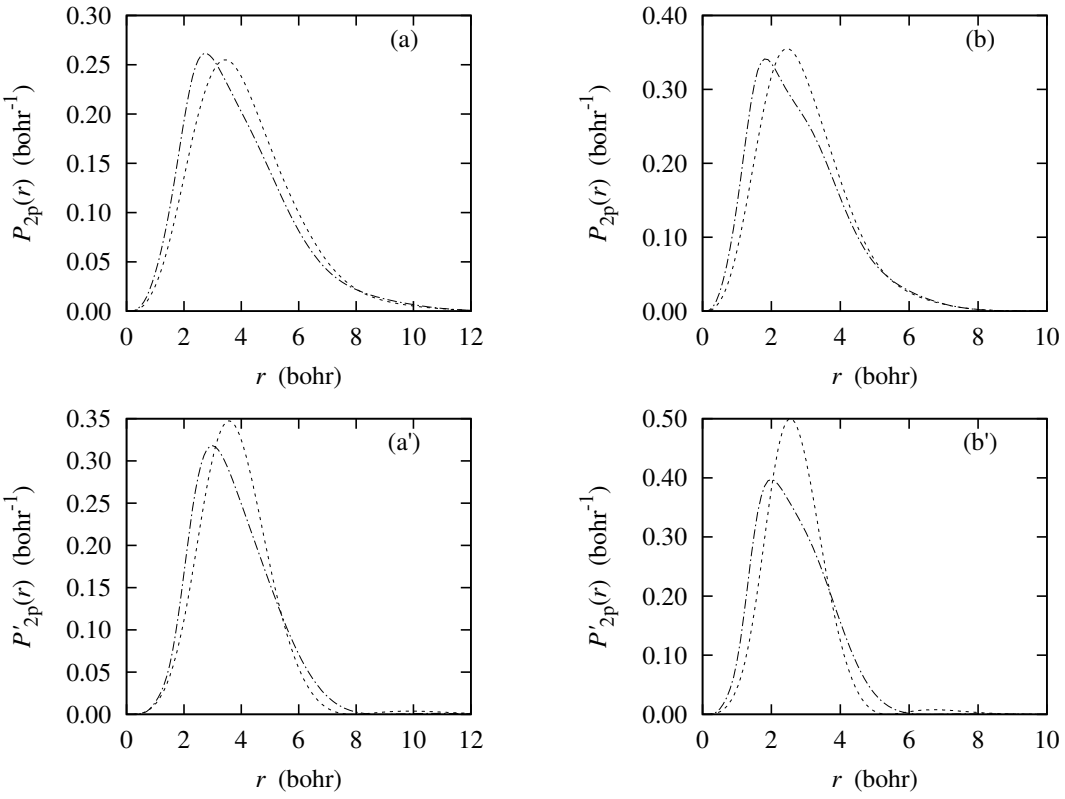

Figure 12. The plots of radial distributions of the correlating $2p$ orbital as a function of r at the CMCSCF with $2s2p$ CAS (- - - - -) and the CMCSCF with $2s2p3s3p3d$ CAS $(-\cdot-\cdot-)$ stationary points for $\eta = \eta_o$ that revealed resonance 1 (a and a′) and resonance 2 (b and b′) .

as indicated in Eq. (4.10) and Eq. (4.15), respectively] of the linear combination,

$$\varphi_{\pm} = \varphi_{\text{res1}} \pm \varphi_{\text{res2}}. \tag{4.19}$$

Notice that the expressions for $P_{\pm}(r)$ and $P'_{\pm}(r)$ remain unaltered if we symmetrically orthogonalize φ_{res1} and φ_{res2} first and then take the linear combination. The minus combination in Figure 13 is vaguely reminiscent of the $2s$ orbital (which may be an artifact of calculation since in actual calculation $3p$ and $4p$ orbitals were found to be resonant orbitals), whereas the other one seems to be a combination of two or more orbitals. As pointed out by Mishra and Venkatnathan,[16] the formation of an electron–atom/molecule scattering resonance is not a single orbital phenomenon, so it is often not easy to say which orbital primarily captures the incoming electron. However, it is clear that the $P_{\pm}(r)$ and $P'_{\pm}(r)$ plots again indicate that there are two ways to form a ^2P Be^- shape resonance — the incoming electron being captured in either of the two resonance orbitals. The label, ^2P is valid for both the cases.

The r_{rms} values for the resonant p orbital from the previous study using direct CMCSCF (∼23.3 and ∼17.7 bohrs for resonances 1 and 2, respectively),[59] are larger than those estimated in M_1 method except for the case of resonance 1 using CSCF. This may be explained by considering the fact that with direct CSCF and CMCSCF the orbitals are actually the "relaxed" orbitals of Be^-. In case of the M_1 method, a CSCF/ CMCSCF Be atom initial state was used where the orbitals are not "relaxed". Moreover, in order to better account for relaxation, all five blocks of the M matrix must be included.[33]

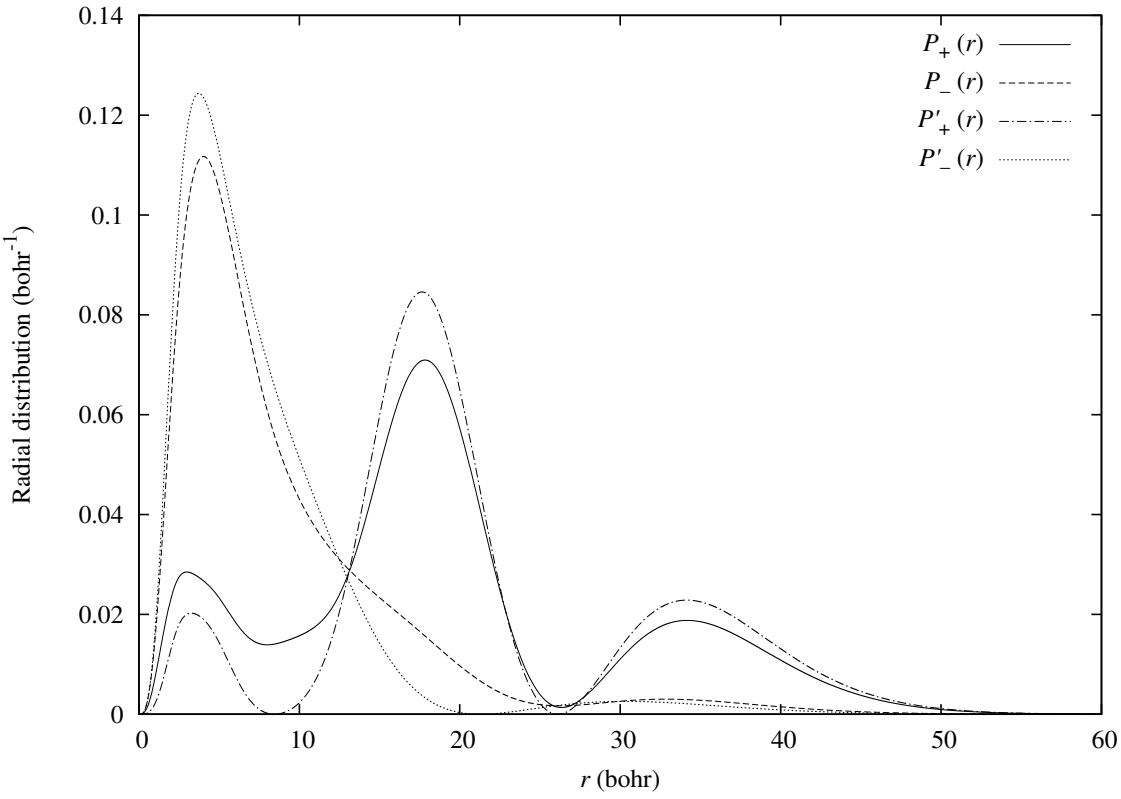

Figure 13. The plots of radial distributions, $P_{\pm}(r)$ and $P'_{\pm}(r)$ of the linear combinations, $\varphi_{\pm} = \varphi_{\rm res1} \pm \varphi_{\rm res2}$, of the two resonance orbitals, $\varphi_{\rm res1}$ and $\varphi_{\rm res2}$ in the CSCF level .

D. Concluding Remarks

In this study we have investigated the ^2P Be^- shape resonances using the M_1 method. This method involves diagonalization of the first block of the M matrix defined for multiconfigurational spin-tensor electron propagator (MCSTEP).[33] The initial state used for the M matrix is the one optimized with the complex multiconfigurational self-consistent field method (CMCSCF) using a non-Hermitian Hamiltonian with electronic coordinates scaled by a complex parameter, $\eta = \alpha \exp(i\theta)$ (α, θ real). We have briefly outlined the underlying theory behind quadratically convergent CMCSCF, which was originally developed by Yeager and Mishra.[50] In this work, we have introduced a new algorithm to control the convergence to the correct CMCSCF stationary point.

The choice of basis set for the Be atom was based on the conclusions of Venkatnathan et al.[57] who after a comprehensive study found $14s11p$ basis to be the best for their single configuration based electron propagator calculations while investigating the same resonance. For the calculations involving $2s2p3s3p3d$ CAS, we augmented this basis set by three uncontracted d functions. The CMCSCF calculations involving various complete active space (CAS) choices, viz. $2s2p$, $2s2p3s$, $2s2p3p$, $2s2p3s3p$ and $2s2p3s3p3d$, and a wide domain of the complex scaling parameters, $0 \leq \theta \leq 0.65$ and $0.60 \leq \alpha \leq 1.10$, have been found to converge with the tolerance of less than 1.0×10^{-10} a.u. for the energy gradient within ten iterations or less. Our calculations show that the M_1 method is a viable and cost-effective method for determining scattering resonance positions and widths.

Our results also show that there are actually two very close–lying ^2P Be^- shape resonances for the scattering of low–energy electrons off a neutral Be target. These two resonances appear in two distinct regions of the continuum of the Hamil-

tonian, and moreover they were unveiled using two very different rotations (η). The wide distribution of resonance energies reported for this particular resonance in the literature may be because of the existence of these two resonances which are very close in energy.

Although the results presented here is solely for atomic shape resonances, the M_1 method may be used for molecular shape resonances as well as for atomic/molecular Auger and Feshbach resonances. For molecular systems, however, the complex electron-nuclear potential energy integrals over basis functions must be calculated for each η using a complex integral evaluation program.

Current work in our laboratory includes combining complex–scaled electron–nuclear attraction integral evaluation subroutine to our CMCSCF codes with application of the M_1 method to study shape, Auger and Feshbach resonances of molecules of chemical and physical interest. In addition, we are developing ways to determine the resonance positions and widths accurately using CMCSCF-based electron propagator method (CMCSTEP) that utilizes the full M matrix, since MCSTEP does not use single determinant based perturbation theory and has been shown to give highly reliable IPs and EAs for atoms and molecules including open shell and highly correlated systems.[33–35,69–75]

CHAPTER V

THE EFFECT OF ORBITALS WITH HIGHER ANGULAR MOMENTUM ON ^2P Be^- SHAPE RESONANCES

A. Introduction

The accuracy of the resonance energy depends on the size of the basis set as well as the method used. For negative ion resonances it is necessary to add enough diffuse functions in the basis set to account for the diffuse nature of the resonance. In addition to that, especially for a multiconfigurational self–consistent field method based on a complex scaled Hamiltonian (CMCSCF),[59] a "balanced" complete active space (CAS) is also very important to determine the resonance energy accurately for the systems with large non-dynamical correlations. An increase in the CAS size by incorporating orbitals with higher angular momentum (e.g., d) increases the number of Slater determinants as well as the number of particle–hole excitations significantly. Apart from increase in computational time required for evaluation of the integrals over a greater number basis functions, a huge number of determinants and particle–hole excitations often lead to computational instability and problem with convergence to the correct CMCSCF stationary point.

The shape resonances are characterized by the "shape" of the angular momentum barrier. So it is interesting to investigate the effect of basis functions with higher angular momentum as well as that of the orbitals with higher angular momentum in the CAS in a CMCSCF calculation. In this study we investigate the effect of systematically building up of bigger CASs that include d functions.

The necessary theoretical background of complex scaling method and CMC-

SCF are given in Chapters II and III. In the next section we present our computational results. At the end we summarize and conclude our discussion.

B. Results and Discussions

1. Computational Details

The basis set for the calculation was the $14s11p3d$ basis set used in Reference 78. The s and p functions were taken from $14s11p$ basis set optimized by Venkatnathan et al.[57] for ^2P Be^- shape resonance. The $14s11p$ basis set was augmented by three uncontracted d functions with coefficients 0.348000, 0.180300 and 0.093414 — first two being from Dunning's pVDZ basis set[76] and the last one added to the set in a geometric progression keeping in mind the diffuse nature of the resonance.

The investigation was started with $2s2p3d$ CAS choice. Similar to our previous calculations,[59] two electrons were placed in the core $1s$ orbital, another two in the partially occupied space and the last electron was placed in a p orbital outside the CAS. The choice of the p orbital which holds the last electron was based on our experience from the M_1 method calculations.[59] The Slater determinants were chosen in such a way that that p orbital was always singly occupied. The rationale came from our previous surmise that the resonance electron for this resonance lies mostly outside the region of the active orbitals.[59] For $\eta = 1$ case for this CAS choice, the initial guess of s and p orbitals were the converged orbitals form the MCSCF ($\eta = 1$ case) calculation[59] with $2s2p$ CAS for the same Be^- state, and the d orbitals were from the MCSCF calculation using the same CAS and the same basis set for the neutral Be atom.

Next, the converged orbitals were taken as the initial guess for CMCSCF calculation with $2s2p3s3d$ and $2s2p3p3d$ CAS choices for the ^2P Be^- states. The resonance final θ–trajectories of the energies of the Be^- states are plotted in Figures 14 and 15 which revealed resonance 1 and resonance 2, respectively. The θ–trajectories for the $2s2p$ CAS is also included for comparison.

2. Resonance Positions and Widths

The positions and widths for the resonance 1 were found to be 0.31 eV and 0.47 eV, 0.30 eV and 0.47 eV, and 0.32 eV and 0.48 eV with $2s2p3d$, $2s2p3p3d$ and $2s2p3s3d$ CAS choices (see Table 6). The respective numbers for resonance 2 were 0.72 eV and 1.54 eV, 0.72 and 1.53 eV, and 0.73 eV and 1.58 eV (see Table 6).

In our previous study,[59] the positions and widths were 0.30 eV and 0.48 eV for resonance 1 and 0.71 eV and 1.56 eV for resonance 2 using $2s2p$ CAS. This indicates that addition of a d orbital to the $2s2p$ CAS changes the position about 3% and the width by 2%. For resonance 2, the change was approximately 1% for each of the position and the width.

The addition of a p orbital to the $2s2p3d$ CAS did not change the resonance energy since it does not provide much correlation, whereas addition of an s function changed the resonance energy a little more which is attributable to the additional "in–out" correlation. This may be attributed to the fact the resonance orbital lies mostly outside of the region of the active orbitals and are more spread–out in space.

Incorporation of d functions causes a significant increase in the number of Slater determinants and particle–hole excitations to be included in a CMCSCF calculation. This in turn results in a higher computational time. Since the resonance positions and widths did not change significantly, the d orbitals in the CAS may not

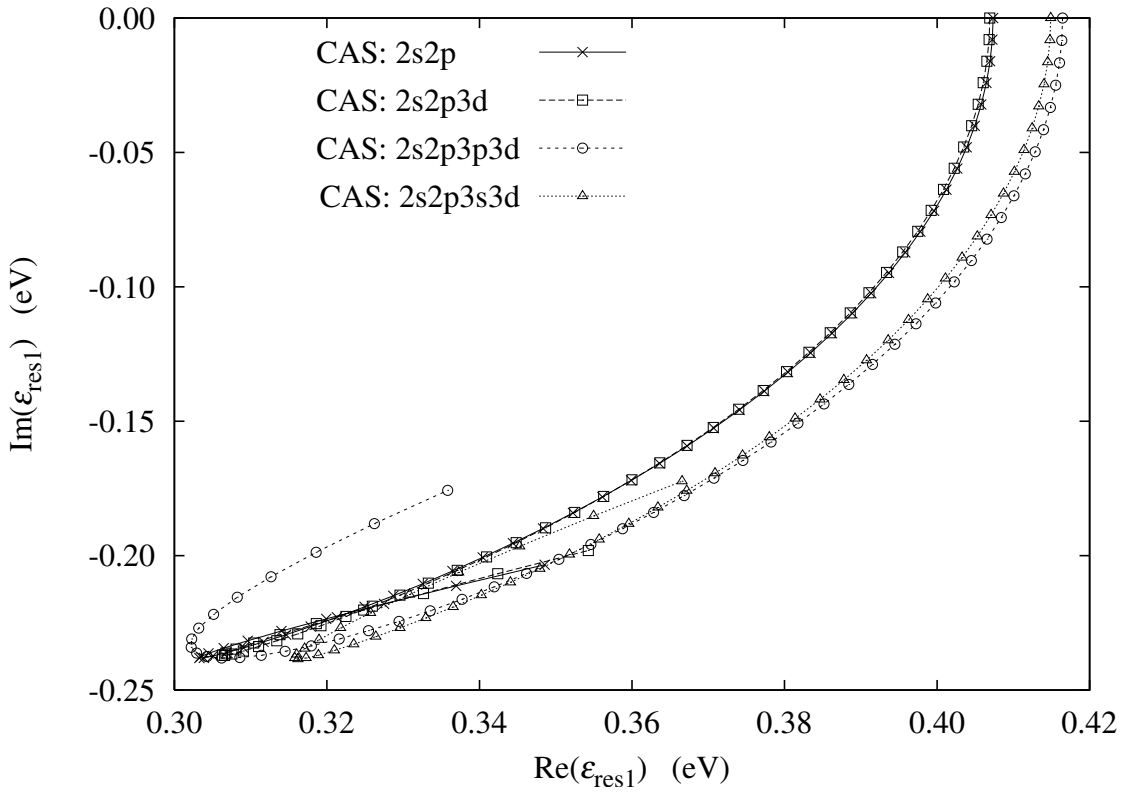

Figure 14. The θ–trajectories for resonance 1 with $2s2p$ ($\alpha_o = 0.980$), $2s2p3d$ ($\alpha_o = 0.980$), $2s2p3p3d$ ($\alpha_o = 0.965$) and $2s2p3s3d$ ($\alpha_o = 0.970$) CAS choices. The trajectories start with $\theta = 0$ at the top where $\mathrm{Im}(\varepsilon_{\mathrm{res1}}) = 0$ and θ is increased linearly in steps of 0.010 rad up to $\theta = 0.500$ rad.

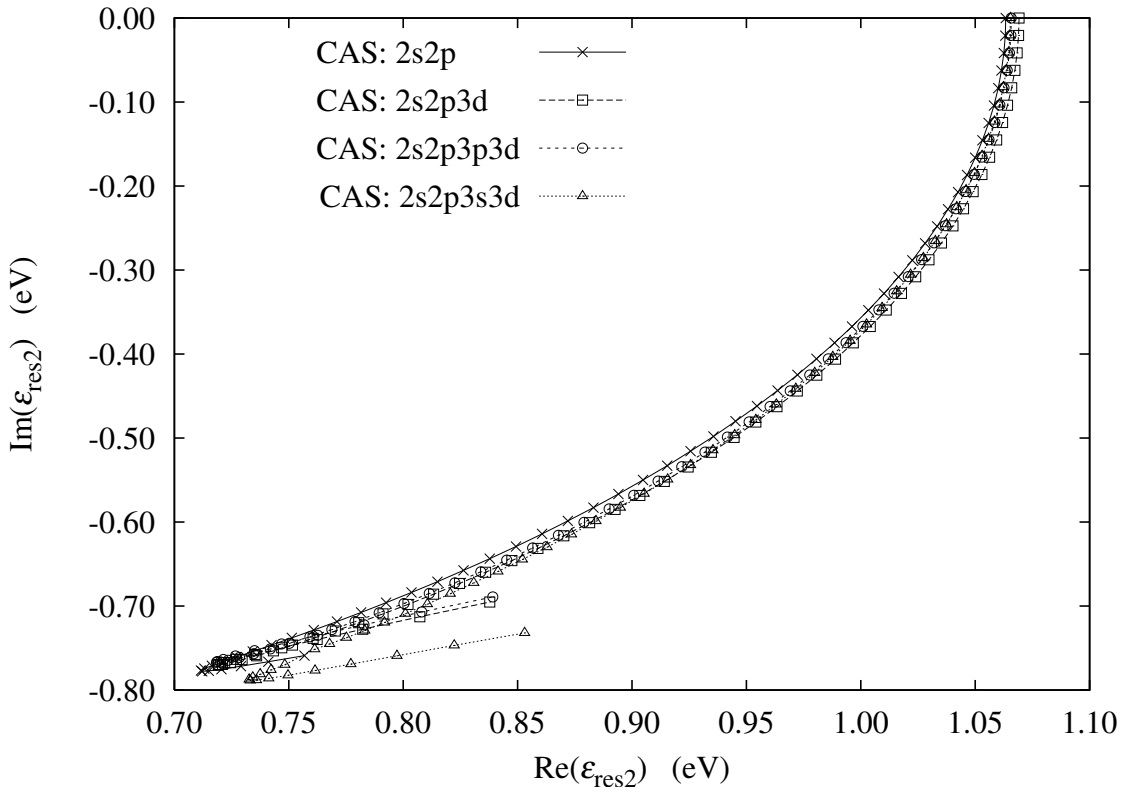

Figure 15. The θ–trajectories for resonance 2 with $2s2p$ ($\alpha_o = 0.985$), $2s2p3d$ ($\alpha_o = 0.980$), $2s2p3p3d$ ($\alpha_o = 0.980$) and $2s2p3s3d$ ($\alpha_o = 0.980$) CAS choices. The trajectories start with $\theta = 0$ at the top where $\mathrm{Im}(\varepsilon_{\mathrm{res1}}) = 0$ and θ is increased linearly in steps of 0.010 rad up to $\theta = 0.580$ rad.

Table 6. Effect of inclusion of a d orbital in the CAS on the resonance positions and widths of the ^2P Be^- shape resonances using CMCSCF.

CAS	Resonance 1		Resonance 2	
	Position (eV)	Width (eV)	Position (eV)	Width (eV)
$2s2p$	0.30	0.48	0.71	1.56
$2s2p3d$	0.31	0.47	0.72	1.54
$2s2p3p3d$	0.30	0.47	0.72	1.53
$2s2p3s3d$	0.32	0.48	0.73	1.58

be necessary to calculate very accurate positions and widths for the ^2P Be^- shape resonances.

C. Concluding Remarks

In this study we addressed an interesting concern about the effect of orbitals of higher angular momentum on the ^2P Be^- shape resonances. In CMCSCF, the effect may be investigated by including, for example, a d orbital in the complete active space (CAS).

We have tested the effect of d orbitals by introducing $2s2p3d$, $2s2p3p3d$ and $2s2p3s3d$ CAS choices. The numbers obtained from our calculations indicate that the incorporation of a d orbital in the CAS has little effect on the resonance energy.

The resonance energy for the first two CAS choices ($2s2p3d$ and $2s2p3p3d$) are very similar and is a little different for the third ($2s2p3s3d$). This indicates that the incorporation of an s orbital has a little more effect than the incorporation of p orbital. The study also indicates that in order to determine very accurate position and width of the ^2P Be^- shape resonances, inclusion of an orbital with higher angular momentum (e.g., d) may not be necessary.

CHAPTER VI

INVESTIGATION OF MOLECULAR RESONANCES USING THE M_1 METHOD BASED ON A CMCSCF REFERENCE STATE

A. Introduction

The successful application of complex scaling technique under the framework of multiconfigurational self-consistent field method to the many–electron atomic resonances prompted us to explore molecular resonances.

The main obstacle in dealing with molecular resonances using complex scaling method (CSM) is that the application of complex scaling theorem for molecular systems is not transparent, especially how to use it vis-à-vis Born–Oppenheimer approximation. In addition to that the electron–nuclear potential is not "dilatation analytic" and the similar scaling of the electronic coordinates results in only an *approximate* complex scaling method.

A summary of the relevant work on how to handle these problems are given in the next section along with appropriate references. Next, our work on $^2\Pi_g$ N_2^- shape resonance using the M_1 method is presented (see Chapter IV for the theory and the working formulas for the M_1 method). At the end we summarized and concluded our discussion on the molecular resonances.

B. Treatment of Molecular Resonances using Complex Scaling Method: Background

The complex scaling method (CSM)[5–7] was originally proposed for one–electron systems and it was later extended to many–electron systems,[9] however, it is not

transparent in the original CSM how it may properly by applied in conjunction with Born-Oppenheimer approximation (BOA) in case of molecular systems. The second problem arises due to the question about the dilatation analiticity of the complex scaled electron–nuclear potential, $V_{\mathrm{en}}(\eta\mathbf{r}, \mathbf{R}_A)$ where

$$V_{\mathrm{en}}(\mathbf{r}, \mathbf{R}_A) = -Z_A|\mathbf{r} - \mathbf{R}_A|^{-1}, \tag{6.1}$$

Z_A is the nuclear positive charge of the atomic center A located at $\mathbf{R}_A$ and η is the complex scale factor which scales the electronic coordinates $\mathbf{r}$ of the Hamiltonian to $\eta\mathbf{r}$ because $V_{\mathrm{en}}(\eta\mathbf{r}, \mathbf{R}_A)$ has square–root branch points along the circle with radius

$$r = |\eta^{-1}|R_A. \tag{6.2}$$

This makes the potential a pathological function of real r with continuous sets of branch points.[79] In addition to that, there were numerical problems[51] while evaluating the integrals of the form

$$\begin{aligned} &\langle\chi_\mu(\mathbf{r}, \mathbf{R}_P)|V_{\mathrm{en}}(\eta\mathbf{r}, \mathbf{R}_A)|\chi_\nu(\mathbf{r}, \mathbf{R}_Q)\rangle \\ &= \eta^{-1}\langle\chi_\mu(\mathbf{r}, \mathbf{R}_P)|V_{\mathrm{en}}(\mathbf{r}, \eta^{-1}\mathbf{R}_A)|\chi_\nu(\mathbf{r}, \mathbf{R}_Q)\rangle, \end{aligned} \tag{6.3}$$

where χ_μ and χ_ν are two arbitrary Gaussian basis functions centered at atomic nuclei P and Q, respectively.

Moiseyev's prescription of applying first the BOA and then the CSM was found to be very useful.[52] Rescigno and McCurdy's[51] as well as Simons'[80] suggestion of incorporating basis functions centered at complex positions, $\eta^{-1}\mathbf{R}_A$ (thus in-

troducing "complex" basis functions), apparently helped circumvent the problem of non-dilatation–analiticity. Moiseyev and Corcoran's idea of rotating the radial path of integration was also a way of avoiding the conceptual problems.[52] It was also suggested that the inclusion of enough diffuse functions may in fact eliminate the need for the complex basis functions.[52,81] Moiseyev showed that the numerical instabilities in evaluating the electron–nuclear integrals only occur for high θ values, where

$$\eta = \alpha \exp i\theta, \quad \alpha \in \mathbb{R}, \theta \in \mathbb{R}. \tag{6.4}$$

In our case, as it will be shown later,

$$\eta_o = \alpha_o \exp(i\theta_o), \tag{6.5}$$

the optimum values of η which revealed the resonances, were very close to unity (hence very small θ) for our calculation of molecular resonances.

The biggest advantage of CSM which has been exploited by the theoreticians in all the complex scaling calculations for atomic resonances is that the integrals over basis functions (or contractions) need to be evaluated only once and these may be used for subsequent calculations with varying η since while evaluating these integrals η may be pulled outside the integral sign. For molecular resonance calculations the same advantage is also present except for the integrals involving $V_{\text{en}}(\mathbf{r}, \eta^{-1}\mathbf{R}_A)$ [see Eq. (6.3)] which need to be evaluated for each η from scratch.

In this study, we used the M_1 method[78] to study $^2\Pi_g$ N_2^- shape resonance within 0-5 eV range, which is probably the most extensively studied molecular resonance in literature.[54,81–90] The results from this study are included in the next section.

C. Results and Discussions

The principal ground–state electronic configuration of N_2 molecule is

$$1\sigma_g^2 1\sigma_u^2 2\sigma_g^2 2\sigma_u^2 1\pi_u^4 3\sigma_g^2.$$

For each value of η, the reference state for $\underline{\underline{M_1}}$ was constructed from the CMCSCF states of ground–state N_2 obtained from the calculations with (1) single configuration CMCSCF (CSCF) and (2) CMCSCF with a p–valence, i.e. $1\pi_u 3\sigma_g 1\pi_g 3\sigma_u$ CAS with eight electrons (PVCAS). The basis set used for this calculation was the economic yet efficient $4s9p$ basis set introduced by Donnelly[81] (see 7). The basis functions are centered at the nitrogen nuclei separated at a distance of 2.068 bohrs. The efficacy of the basis set was verified by Mishra et al.[54,88–90]

The orbital energies of the lowest three molecular orbitals (MOs) of N_2 with π_g symmetry were found to be 0.673, 2.101 and 3.580 eV from an SCF calculation ($\eta = 1$). In order to see which one of these is (are) the potential resonance root(s), the "electron affinities" (EAs) of these three virtual orbitals were calculated using the M_1 method with CSCF reference states at a series of θ values holding α constant at unity. It was found that only the second root shows proper stability at around $\theta = 0.30$ rad. This was further verified using the M_1 method with PVCAS reference state.

Next, the EAs corresponding to the resonance orbital were calculated for different α and θ values using the M_1 method with CSCF as well as PVCAS reference states. Then several θ–trajectories were plotted at a series of constant α values. The θ–trajectories showing the sharpest cusps are shown in Figure 16. The resonance positions and the widths obtained from the stabilization observed in the θ–trajectories

Table 7. The $(9s, 11p) \rightarrow [4s, 9p]$ basis set for nitrogen used in this work.[81]

Index	Type	Exponents	Coefficients
1	s	5909.4400000	0.0020040
		887.4510000	0.0153100
		204.7490000	0.0742930
		59.8376000	0.2533640
		19.9981000	0.6005760
		2.6860000	0.2451110
2	s	7.1927000	1.0000000
3	s	0.7000000	1.0000000
4	s	0.2133000	1.0000000
1	p	26.7860000	0.0382440
		5.9564000	0.2438460
		1.7074000	0.8171930
2	p	0.5314000	1.0000000
3	p	0.1654000	1.0000000
4	p	0.6000000	1.0000000
5	p	0.2600000	1.0000000
6	p	0.1250000	1.0000000
7	p	0.0500000	1.0000000
8	p	0.0200000	1.0000000
9	p	0.0080000	1.0000000

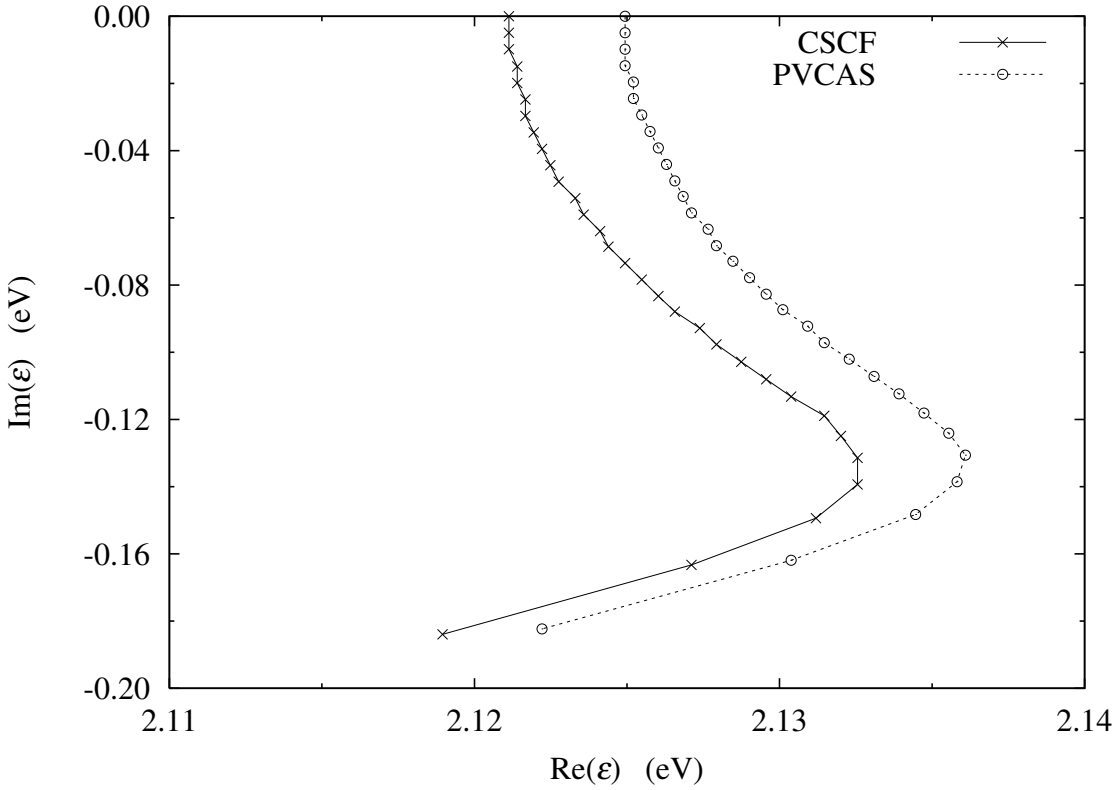

Figure 16. The θ–trajectories for the EAs (ε) corresponding to the $^2\Pi_g$ N_2^- resonance root from the M_1 method calculations using CSCF and PVCAS reference states . The θ–trajectories start with $\theta = 0$ at the top where Im(ε)=0 and incremented linearly in steps of 1.0×10^{-3} rad up to $\theta = 0.03$ rad. The other parameter, α was held constant at its optimum value, $\alpha_o = 0.995$ (same for both trajectories).

in Figure 16 are listed in Table 8 along with previously reported numbers. The resonance positions and widths from this calculation were 2.13 eV and 0.27 eV, and 2.14 eV and 0.27 eV for CSCF and PVCAS, respectively.

An important feature to notice is that on going from CSCF reference state to a CMCSCF one the resonance position and width hardly changed. This is again an indication that the resonance orbital lies away from the region of the active orbitals.

Our numbers are in excellent agreement with those obtained from the dilated electron propagator (EP) calculations by Donnelly[81] as well as Mishra et al.[54,88–90] The resonance positions obtained from this study are very close to experimental value of 2.20 eV, although the width is slightly low compared to the experiment (0.57 eV).

It is interesting to notice that the the rotation required to unveil the $^2\Pi_g$ N_2^- shape resonance was very close to unity ($\alpha_o = 0.995, \theta_o \sim 0.030$ rad), which is similar to the observation by Donnelly[81] and Mishra et al.[54,88–90] This indicates that even for a moderately sized basis set the M_1 method is an effective tool to study resonances. This being our first application of a CMCSCF–based method to study a molecular resonance, a few words about convergence is necessary. Similar to the case of atomic resonances,[59,78] in case of almost all the η values explored, the CMCSCF calculation converged within ten iterations or less within a tolerance of 1.0×10^{-10} a.u. for the energy gradient. The computational times required for each CMCSCF calculation was similar to the atomic CAS with a similar CAS size. However, overall time for exploring different η values is slightly longer because of the need to calculate the electron–nuclear integrals for each η.

Table 8. $^2\Pi_g$ N_2^- shape resonance positions and widths from experiment, previous theoretical work and this work.

Method	Position (eV)	Width (eV)
Experiment[91]	2.20	0.57
Static exchange[92]	3.70	1.16
Static exchange R-matrix[84]	2.15	0.34
Stabilization method[93]	2.44	0.32
R-matrix[84]	3.26	0.80
Many-body optical potential[86,94]	3.80	1.23
Boomerang model[95]	1.91	0.54
Stieltjes imaging technique[96]	4.13	1.14
Complex SCF[85]	3.19	0.44
Second order dilated EP (real SCF)[81]	2.14	0.26
Zeroth order biorthogonal dilated EP[88]	2.07	0.14
Second order biorthogonal dilated EP[90]	2.11	0.18
Third order biorthogonal dilated EP[90]	2.11	0.18
M_1 method with CSCF reference state (*this work*)	2.13	0.27
M_1 method with PVCAS reference state (*this work*)	2.14	0.27

D. Concluding Remarks

The problems associated with dealing with molecular resonances using complex scaling method (CSM) as well as a summary of relevant development in this field have been discussed. The application of of CSM along with Born–Oppenheimer approximation (BOA) is complicated and an approximation solution can be achieved by first applying the BOA and then the CSM following Moiseyev and Corcoran's suggestion.[52] As a remedy to the problem of non-dilatation-analiticity of the electron–nuclear potential, enough diffuse functions were included in the basis set.[81]

We applied the M_1 method which is based on a complex multiconfigurational self-consistent field (CMCSCF) reference state with a p–valence, i.e. $1\pi_u 3\sigma_g 1\pi_g 3\sigma_u$CAS (PVCAS) to calculate the resonance energy of $^2\Pi_g$ N_2^- shape resonance. The resonance position and width were found to be 2.14 and 0.27 eV, respectively. In order to see the effect of non-dynamic correlation accounted for by the application of the M_1 method based on the PVCAS, we also calculated the resonance position (2.13 eV) and width (0.27 eV) using a single reference based CMCSCF (i.e., CSCF). It is evident the the resonance position and width did not change much on going from CSCF to CMCSCF.

This work on molecular resonances establishes that CMCSCF/M_1 method is a viable and cost–effective method in the investigation of resonances. This work will be followed up with the investigation of other chemically and physically interesting atomic and molecular resonances.

CHAPTER VII

SUMMARY AND CONCLUSIONS

This investigation involves development, implementation and application of multiconfigurational self-consistent field method (MCSCF) based approach to study electron–atom/molecular scattering resonances utilizing the complex scaling method (CSM).[5–7]

The resonances are metastable states which lie in the continuum part of the Hamiltonian. But the application of CSM makes the study of these temporarily bound states amenable to bound–state electronic structure methods. The resonant wavefunction may be expressed as $\Psi(\mathbf{r},t) = \psi(\mathbf{r})\exp(-iEt/\hbar)$ where the energy E is a complex number with real part equal to the position (E_r) and twice the absolute value of its imaginary part equal to the width (Γ) of the resonance. Γ is related to its life–time (τ) by the uncertainty relation: $\Gamma = \hbar/\tau$. In regular quantum mechanics, the Hamiltonian is Hermitian, and so it cannot have complex eigenvalues. As a consequence of that resonances stay "hidden" in the continuum part of the Hamiltonian. The CSM, which is essentially scaling of the electronic coordinates ($\mathbf{r}$) of the Hamiltonian by a complex scale factor, $\eta = \alpha\exp(i\theta)$ (α and θ real), as $\mathbf{r} \rightarrow \eta\mathbf{r}$, causes the continuum of the Hamiltonian rotate by an angle -2θ and exposes the resonances hidden in the continua as the continuum rays are made to pass through them by varying θ. A brief overview of the CSM and the complex scaling transformation along with its implications, viz. non-Hermiticity of the complex scaled Hamiltonian, biorthogonality of the eigenfunctions of the complex scaled Hamiltonian and the appearance of complex eigenvalues were outlined in the first chapter. This chapter also includes discussion on how to evaluate the complex integrals in order to

construct the complex scaled Hamiltonian.

In the next chapter we outlined the development of the quadratically convergent MCSCF scheme using a complex scaled Hamiltonian (CMCSCF). It was observed that the CMCSCF equations look exactly the same as the ones for MCSCF, which made it very easy to modify the existing MCSCF code to adapt it for CMCSCF calculations.[50,59] The real MCSCF program uses an efficient step–length control algorithm to converge to the correct stationary point.[36] A similar algorithm has been suggested which facilitates convergence for CMCSCF calculations.

The CMCSCF method was applied to study the resonance positions and widths of ^2P Be^- shape resonances using different complete active space (CAS) choices, e.g. $2s2p$, and $2s2p3s3p$. Another calculation using CMCSCF with a single determinantal wavefunction which mimics bivariational SCF (CSCF) was also performed in order to see the effect of introducing better CASs. The basis set for all these calculations was $14s11p$ which was found by Venkatnathan et al.[57] to be the best–suited for this resonance.

We obtained two distinct low–lying resonances ("resonance 1" and "resonance 2") with ^2P symmetry from the CMCSCF calculation, which are very close in energy. The previous calculations done on this resonance revealed only one of these (see 3), but there is a wide distribution of the resonance positions and widths reported. The wide range of these numbers may be explained if we consider the existence of the two resonances revealed in this calculation. The resonance positions and widths from the CMCSCF calculation with the biggest CAS choice ($2s2p3s3p$) was found to be 0.32 eV and 0.49 eV for resonance 1 and 0.73 eV and 1.58 eV for resonance 2, respectively. The radial distribution plots of the resonance orbitals indicate that correlation and relaxation effects are important for this resonance. For all the CAS choices and various different values of the complex scale factor (η), the CMCSCF convergence

was quite fast – the calculations converged with a tolerance of 1.0×10^{10} a.u. for the energy gradient within ten iterations or less.

In the next chapter we introduced the M_1 method based on a CMCSCF reference state. This uses the first block of the M matrix, ($\underline{\underline{M_1}}$) defined in the multiconfigurational spin–tensor electron propagator method (MCSTEP)[33] except for the fact that $\underline{\underline{M_1}}$ uses a complex scaled Hamiltonian and the operators correspond to a set of biorthogonal spin orbitals. We used the M_1 method to study ^2P Be^- shape resonances using different CMCSCF reference states with $2s2p$, $2s2p3s$, $2s2p3p$, $2s2p3s3p$ and $2s2p3s3p3d$ CAS choices as well as a CSCF reference state using a single determinantal wavefunction. For CSCF and the CMCSCF calculations with no d orbital in the CAS, the same $14s11p$ basis set[57] was used. For the remaining CAS choice, this basis set was augmented with three even–tempered d–type functions — first two of which came from Dunning's pVTZ basis set and third was added to this set in a geometric progression keeping in mind the diffuse nature of the resonance.

The M_1 method also revealed two low–lying resonances for ^2P Be^- shape resonances which are very close in energy. The resonance position and width from the M_1 method calculation where the CMCSCF ground state with the largest CAS ($2s2p3s3p3d$) was chosen as the reference state for $\underline{\underline{M_1}}$ were found to be 0.57 eV and 1.19 eV for resonance 1 and 0.72 eV and 1.12 eV for resonance 2, respectively.

In order to visualize the resonance orbitals, the "radial distribution" [see Eq. (4.10) and (4.15)] of the resonance orbital was plotted along with other orbitals in the CAS. The resonance orbitals has unique features compared with other orbitals (see Figures 10–13). The expectation values of r^2 indicate that the resonance orbitals lie further away from the region of the active orbitals.

This study on ^2P Be^- proves that M_1 method is a very efficient and cost effective method in investigating scattering resonances. However, the orbitals included

in this calculation are the neutral Be orbitals and so they are not relaxed. Moreover, as MCSTEP calculations show that the other blocks of the M matrix, in addition to the first, be included for accurate ionization and electron attachment energies for highly correlated systems.[33–35,69–75] However, the development and implementation of M_1 method serves as an important stepping stone toward the development of complex MCSTEP (CMCSTEP) that uses a complex scaled Hamiltonian.

In order to verify that these two resonances are indeed distinct, we plotted the radial distributions of the simple "+" and the "−" linear combinations of the resonance orbitals [see Eq. (4.19). Had the two been the same they would have cancel each other in the region of spatial contiguity (see Figure 13). However, the plot for "−" combination look a lot like a $2p$ orbital whereas the and "+" combination is similar to a combination of $4p$ and some other orbital. This indicates that the resonances are distinct. This also indicates that these resonances may not be described as "single orbital" phenomena.

The shape resonances are characterized by the "shape" of the angular momentum barrier. So, in our next study we made an effort to see how the incorporation of orbitals of higher angular momentum (e.g., d) in the CAS affect the resonance positions and the widths. For a MCSCF/CMCSCF calculation, an increase in the CAS size increases numerical complexity and gives rise to convergence problems besides increasing the computational cost in general. We used the direct CMCSCF method (see Chapter III) to investigate the effect of incorporation of a d orbital in the CAS. Similar to the method outlined in Chapter III we studied various ^2P states of Be^- in order to see which ones show resonance characteristics. This revealed that there are actually two low–lying resonances which are very close in energy similar to our observation in Chapters III and IV). We first investigated the effect of adding a d orbital to the smallest $2s2p$ CAS. Next we added an s function to the resultant CAS

($2s2p3d$) to form a $2s2p3s$ CAS. On another calculation we added a s orbital to the $2s2p3d$ CAS. The $2s2p3d$ CAS did not show much change in the positions and widths. The second CAS, $2s2p3p$ CAS also did not show much change. A little more change was observed in case of $2s2p3s3d$ CAS which may be attributed to the better "in–out" correlation. However, the change due to the addition of an extra d function was not big and this lead us to conclude that the addition of a d orbital was not necessary for obtaining "better" resonance positions and widths for these low–lying ^2P Be^- shape resonances. However, this analysis revealed that the resonance energy may be obtained with high accuracy even without including the d functions in the CAS and thus computational cost may be minimized.

After successfully implementing the CMCSCF based methods for atomic resonance, we moved on to investigate molecular resonances. However, for molecular resonances the application of CSM is not very straightforward because of the involvement of the nuclear motion along with the electronic motion. Moreover, the complex scaled electron is not dilatation analytic which results in conceptual problems in application of the CSM. However, we followed Moiseyev and Corcoran's prescription[52] of dealing with the problem with the integrals involving the electron–nuclear potential. We applied the M_1 method (see Chapter IV) based on the CMCSCF reference state with a p–valence, i.e. $1\pi_u 3\sigma_g 1\pi_g 3\sigma_u$ CAS, to calculate resonance positions and widths of the $^2\Pi_g$ N_2^- shape resonance within 0–5 eV range. In order to compare with bivariational SCF results we also used M_1 method based on the CSCF reference state. We chose $4s9p$ basis set first proposed by Donnelly.[81] The best values for the position and widths of these resonances were found to be 2.14 eV and 0.27 eV, which are very close to experimental and other electron–propagator based methods.

The development and implementation of CMCSCF is an important progress in understanding the scattering resonances from a bound–state point of view. Al-

though we presented the calculations for two shape resonances, viz. ^2P Be^- and $^2\Pi_g$ N_2^- shape resonances, the CMCSCF and the M_1 method may be applied to study Auger and Feshbach resonances as well. Multiconfigurational–based methods have an established history of accurate calculation of properties of highly correlated systems.[29,30,33–35,37,58,59,69–75,78] In future the other chemically and physically interesting atomic or molecular resonances will be explored using CMCSCF and M_1 method. This implementation of MCSCF using CSM paves the way to develop more accurate CMCSCF based, e.g. multiconfigurational spin–tensor electron propagator (MCSTEP) using a complex scaled Hamiltonian, which will enable one to investigate scattering resonances with a higher degree of accuracy.

REFERENCES

(1) Bardsley, J. N.; Biondi, M. A. *Adv. Atom. Mol. Phys.* **1971**, *6*, 1.

(2) Massey, H. *Negative Ions*, 3rd ed.; Cambridge University Press: Cambridge, UK, 1976.

(3) Barrios, R.; Skurski, P.; Simons, J. *J. Phys. Chem. B* **2003**, *106*, 7991–7994.

(4) Hazi, A. U.; Taylor, H. S. *Phys. Rev. A* **1970**, *1*, 1109–1120.

(5) Aguilar, J.; Combes, J. M. *Commun. Math. Phys.* **1971**, *22*, 269–279.

(6) Balslev, E.; Combes, J. M. *Commun. Math. Phys.* **1971**, *22*, 280–294.

(7) Simon, B. *Commun. Math. Phys.* **1972**, *27*, 1–9.

(8) Simon, B. *Int. J. Quantum Chem.* **1978**, *14*, 529–542.

(9) Rescigno, T. N.; McCurdy, J. C. W.; Orel, A. E. *Phys. Rev. A* **1978**, *17*, 1931–1938.

(10) Moiseyev, N.; Certain, P. R.; Weinhold, F. *Int. J. Quantum Chem.* **1978**, *14*, 727–736.

(11) Mishra, M. K.; Goscinski, O.; Öhrn, Y. *J. Chem. Phys.* **1983**, *79*, 5505–5511.

(12) Lucchese, R. R.; Takatsuka, K.; McKoy, V. *Phys. Rep.* **1986**, *131*, 147–221.

(13) Löwdin, P.-O.; Froelich, P.; Mishra, M. *Adv. Quantum Chem.* **1989**, *20*, 185–237.

(14) Riss, U. V.; Meyer, H. D. *J. Phys. B* **1993**, *26*, 4503–4536.

(15) Moiseyev, N. *Phys. Rep.* **1998**, *302*, 211–293.

(16) Mishra, M. K.; Venkatnathan, A. *Int. J. Quantum Chem.* **2002**, *90*, 1334–1347.

(17) Santra, R.; Cederbaum, L. S. *J. Chem. Phys.* **2002**, *117*, 5511–5521.

(18) Sajeev, Y.; Santra, R.; Pal, S. *J. Chem. Phys.* **2005**, *123*, 204110–1–204110–10.

(19) Vaval, N.; Cederbaum, L. S. *J. Chem. Phys.* **2007**, *126*, 164110–1–164110–6.

(20) Taylor, H. S.; Hazi, A. U. *Phys. Rev. A* **1976**, *14*, 2071–2074.

(21) Liebman, J. F.; Yeager, D. L.; Simons, J. *Chem. Phys. Lett.* **1977**, *48*, 227–232.

(22) Lipkin, N.; Moiseyev, N.; Brändas, E. *Phys. Rev. A* **1989**, *40*, 549–553.

(23) Rom, N.; Brändas, E.; Moiseyev, N. *J. Chem. Phys.* **1990**, *93*, 3413–3419.

(24) Simon, B. *Phys. Lett.* **1979**, *71A*, 211–214.

(25) McCurdy, C. W.; Rescigno, T. N.; Davidson, E. R.; Lauderdale, J. G. *J. Chem. Phys.* **1980**, *73*, 3268–3273.

(26) Riss, U. B.; Meyer, H. D. *J. Phys. B* **1998**, *31*, 2279–2304.

(27) Moiseyev, N. *J. Phys. B* **1998**, *31*, 1431–1441.

(28) Sommerfeld, T.; Riss, U. V.; Meyer, H. D.; Cederbaum, L. S.; Engels, B.; Suter, H. U. *J. Phys. B* **1998**, *31*, 4107–4122.

(29) Yeager, D. L.; Jørgensen, P. *J. Chem. Phys.* **1979**, *71*, 755–760.

(30) Jørgensen, P.; Simons, J. *Second Quantization-Based Methods in Quantum Chemistry*; Academic Press: New York, 1981.

(31) Olsen, J.; Yeager, D. L.; Jørgensen, P. *Adv. Chem. Phys.* **1983**, *54*, 1–176.

(32) Graham, R.; Yeager, D. L.; Olsen, J.; Jørgensen, P.; Harrison, R.; Zarrabian, S.; Bartlett, R. *J. Chem. Phys.* **1986**, *85*, 6544–6549.

(33) Golab, J. T.; Yeager, D. L. *J. Chem. Phys.* **1987**, *87*, 2925–2944.

(34) Graham, R. L.; Yeager, D. L.; Rizzo, A. *J. Chem. Phys.* **1989**, *91*, 5451–5454.

(35) Rizzo, A.; Yeager, D. L. *J. Chem. Phys.* **1990**, *93*, 8011–8020.

(36) Jørgensen, P.; Swanstrøm, P.; Yeager, D. L. *J. Chem. Phys.* **1983**, *78*, 347–356.

(37) Yabushita, S.; McCurdy, C. W. *J. Chem. Phys.* **1985**, *83*, 3547–3559.

(38) Siegert, A. J. F. *Phys. Rev.* **1939**, *56*, 750–752.

(39) Dirac, P. *Proc. Roy. Soc. London* **1927**, *A14*, 243.

(40) Dirac, P. *The Principles of Quantum Mechanics*; Clarendon Press: Oxford, 1958.

(41) Gamow, G. *Constitution of Atomic Nuclei and Radioactivity*; Oxford University Press: Oxford, 1931.

(42) Simons, J. *Int. J. Quantum Chem.* **1981**, *20*, 779–780.

(43) Bardsley, J. N. *Int. J. Quantum Chem.* **1978**, *14*, 343–352.

(44) Löwdin, P.-O.; Froelich, P.; Mishra, M. *Adv. Quantum Chem.* **1988**, *19*, 87–138.

(45) Löwdin, P.-O.; Froelich, P.; Mishra, M. K. *Int. J. Quantum Chem.* **1989**, *36*, 93–103.

(46) Brändas, E.; Froelich, P. *Phys. Rev. A* **1977**, *16*, 2207–2210.

(47) Löwdin, P.-O. *J. Math. Phys.* **1983**, *24*, 70–87.

(48) Moiseyev, N. *Phys. Rev. A* **1981**, *24*, 2824–2825.

(49) Mishra, M.; Goscinski, O.; Öhrn, Y. *J. Chem. Phys.* **1983**, *79*, 5494–5504.

(50) Yeager, D. L.; Mishra, M. K. *Int. J. Quantum Chem.* **2005**, *104*, 871–879.

(51) McCurdy, C. W., Jr.; Rescigno, T. N. *Phys. Rev. Lett.* **1978**, *41*, 1364–1368.

(52) Moiseyev, N.; Corcoran, C. *Phys. Rev. A* **1979**, *20*, 814–817.

(53) Donnelly, R. A. *J. Chem. Phys.* **1986**, *84*, 6200–6203.

(54) Medikeri, M. N.; Mishra, M. K. *Chem. Phys. Lett.* **1995**, *246*, 26–32.

(55) Venkatnathan, A.; Mishra, M. K. *Chem. Phys. Lett.* **1998**, *296*, 223–232.

(56) Mahalakshmi, S.; Mishra, M. K. *Chem. Phys. Lett.* **1998**, *296*, 43–50.

(57) Venkatnathan, A.; Mishra, M. K.; Jensen, H. J. A. *Theor. Chem. Acc.* **2000**, *104*, 445–454.

(58) Yeager, D. L.; Albertsen, P.; Jørgensen, P. *J. Chem. Phys.* **1980**, *73*, 2811–2816.

(59) Samanta, K.; Yeager, D. L. *J. Phys. Chem. B* **2008**, *112*, 16214–16219.

(60) Fletcher, R. *Practical Methods of Optimization*; Wiley: New York, 1980.

(61) Huzinaga, S. *J. Chem. Phys.* **1965**, *42*, 1293–1302.

(62) Kurtz, H. A.; Öhrn, Y. *Phys. Rev. A* **1979**, *19*, 43–48.

(63) Kurtz, H. A.; Jordan, K. D. *J. Phys. B* **1981**, *14*, 4361–4376.

(64) McNutt, J. F.; McCurdy, C. W. *Phys. Rev. A* **1983**, *27*, 132–140.

(65) Krylstedt, P.; Rittby, M.; Elander, N.; Brändas, E. *J. Phys. B* **1987**, *20*, 1295–1327.

(66) Krylstedt, P.; Rittby, M.; Elander, N.; Brändas, E. *J. Phys. B* **1988**, *21*, 3969–3988.

(67) Donnelly, R. A.; Simons, J. *J. Chem. Phys.* **1980**, *73*, 2858–2866.

(68) McCurdy, C. W.; McNutt, J. F. *Chem. Phys. Lett.* **1983**, *94*, 306–310.

(69) Yeager, D. L. In *Applied Many-Body Methods in Spectroscopy and Electronic Structure*; Mukherjee, D., Ed.; Plenum: New York, 1992; p 133.

(70) Yeager, D. L. *Trends Chem. Phys.* **1999**, *7*, 65–86.

(71) Mahalakshmi, S.; Yeager, D. L. *Mol. Phys.* **2003**, *100*, 3743.

(72) Mahalakshmi, S.; Yeager, D. L. In *Fundamental World of Quantum Chemistry: A Tribute to Per-Olov Löwdin*; Brändas, E. J., Kryachko, E. S., Eds.; Kluwer Academic Publishers: Dordrecht, 2004; Vol. III, p 547.

(73) Saha, R.; Ma, D.; Yeager, D. L. *Int. J. Quantum Chem.* **2007**, *107*, 694–702.

(74) Ma, D.; Yeager, D. L. *Int. J. Quantum Chem.* **2008**, *108*, 100–101.

(75) Ma, D.; Yeager, D. L. *Int. J. Quantum Chem.* **2008**, *108*, 1130–1136.

(76) Dunning, T. H. *J. Chem. Phys.* **1989**, *90*, 1007–1023.

(77) Langhoff, S. R.; Davidson, E. R. *Int. J. Quantum Chem.* **1974**, *8*, 61.

(78) Samanta, K.; Yeager, D. L. *Int. J. Quantum Chem.* **2009**, *in press.*

(79) McCurdy, C. W. *Phys. Rev. A* **1980**, *21*, 464–470.

(80) Simons, J. *J. Chem. Phys.* **1980**, *73*, 992–993.

(81) Donnelly, R. A. *Int. J. Quantum Chem. Symp.* **1982**, *16*, 653–659.

(82) Krauss, M.; Mies, F. H. *Phys. Rev. A* **1970**, *1*, 1592.

(83) Schultz, G. J. In *Principles of Laser Plasmas*; Bekefi, G., Ed.; Wiley: New York, 1976.

(84) Schneider, B.; LeDourneuf, M.; Lan, V. K. *Phys. Rev. Lett.* **1979**, *43*, 1926.

(85) Rescigno, T. N.; Orel, A. E. *J. Chem. Phys.* **1980**, *73*, 6347–6348.

(86) Meyer, H. D. *Phys. Rev. A* **1989**, *40*, 5605.

(87) Mishra, M. K.; Medikeri, M. N. *Adv. Quantum Chem.* **1996**, *27*, 223.

(88) Medikeri, M. N.; Mishra, M. K. *Int. J. Quantum Chem. Symp.* **1994**, *28*, 29–37.

(89) Mahalakshmi, S.; Mishra, M. K. *Indian J. Chem.* **2000**, *39A*, 22–31.

(90) Mahalakshmi, S.; Venkatnathan, A.; Mishra, M. K. *J. Chem. Phys.* **2001**, *115*, 4549–4557.

(91) Schultz, G. J. *Rev. Mod. Phys.* **1970**, *45*, 379.

(92) Schneider, B. I. *Phys. Rev. A* **1981**, *24*, 1.

(93) Chao, J. S.-Y.; Falcetta, M. F.; Jordon, K. D. *J. Chem. Phys.* **1990**, *93*, 1125.

(94) Berman, M.; Walter, O.; Cederbaum, L. S. *Phys. Rev. Lett.* **1983**, *50*, 1979.

(95) Dube, L.; Herzenberg, A. *Phys. Rev. A* **1979**, *20*, 194.

(96) Hazi, A. U.; Rescigno, T. N.; Kurilla, M. *Phys. Rev. A* **1981**, *23*, 1089.

VITA

Kousik Samanta was born in India in 1981. He obtained a Bachelor of Science (B.Sc.) with honors in chemistry from the University of Calcutta, India in 2001. He worked with Professor Manoj K. Mishra at Indian Institute of Technology, Bombay, India as a graduate student, where he obtained a Master of Science (M.Sc.) in chemistry with a specialization in physical chemistry in 2003. Then he moved to Texas A&M University to start his graduate studies under the supervision of Professor Danny L. Yeager. He graduated with a Ph.D. in chemistry in May 2009.

Kousik may be reached through the Department of Chemistry, Texas A&M University, College Station, TX 77843, USA. His email address is kousik@tamu.edu.